



1 **Modelling evaporation with local, regional and global BROOK90** 2 **frameworks: importance of parameterization and forcing.**

3 Ivan Vorobevskii, Thi Thanh Luong, Rico Kronenberg, Thomas Grünwald, Christian Bernhofer

4 Faculty of Environmental Sciences, Department of Hydrosociences, Institute of Hydrology and Meteorology, Chair of
5 Meteorology, Technische Universität Dresden, Tharandt, 01737, Germany

6 *Correspondence to:* Ivan Vorobevskii (ivan.vorobevskii@tu-dresden.de)

7

8 **Abstract.**

9 Observation and estimation of evaporation is a challenging task. Evaporation occurs on each surface and is driven by
10 different energy sources. Thus the correct process approximation in modelling of the terrestrial water balance plays a crucial
11 part. Here, we use a physically-based 1D lumped soil-plant-atmosphere model (BROOK90) to study the role of parameter
12 selection and meteorological input for modelled evaporation on the point scale. Then, with the integration of the model into
13 global, regional and local frameworks, we made cross-combinations out of their parameterization and forcing schemes to
14 analyse the associated model uncertainty.

15 Five sites with different land uses (grassland, cropland, deciduous broadleaf forest, two evergreen needleleaf forests) located
16 in Saxony, Germany were selected for the study. All combinations of the model setups were validated using FLUXNET data
17 and various goodness of fit criteria. The output from a calibrated model with in-situ meteorological measurements served as
18 a benchmark. We focused on the analysis of the model performance with regard to different time-scales (daily, monthly, and
19 annual). Additionally, components of evaporation are addressed, including their representation in BROOK90. Finally, all
20 results are discussed in the context of different sources of uncertainty: model process representation, input meteorological
21 data and evaporation measurements themselves.

22 **1 Introduction**

23 Evaporation as a water balance component plays an important role in the hydrological process at multiple spatial scales:
24 from a single leaf to an entire catchment. As a result of mass and energy exchange between the soil-plant and atmosphere
25 system, the global annual terrestrial evaporation amount yields approximately $\frac{2}{3}$ of the total precipitation. However, with the
26 need of higher spatial and temporal resolution, evaporation exposes larger variability (Jung et al., 2011; Zhang et al., 2010;
27 Pan et al., 2020; Baldocchi et al., 2001; Anderson et al., 2007). Thus, accurate estimates of evaporation on different scales as
28 well as deepening knowledge of the process itself, are beneficial for planning, developing and monitoring of hydrologic,
29 agriculture and ecological systems, e.g., irrigation scheduling, water distribution systems, crop modelling, quantification of



30 energy and moisture exchange between the land surface and the atmosphere (McNally et al., 2019; Schulz et al., 2021;
31 Fisher et al., 2017). Apart from the total evaporation itself, it is sometimes necessary to assess and quantify its components
32 (Lawrence et al., 2007; Schulz et al., 2021; Leuning et al., 2008; Chang et al., 2018), namely components, like transpiration,
33 evaporation from the ground or snow surface, and evaporation of intercepted rain and snow from the canopy.

34 Various direct (i.e. porometer, eddy-covariance lysimeter) and indirect (Bowen ratio, gradient, experimental water balance
35 watersheds) methods have been developed and used to measure evaporation at different spatio-temporal scales. Each method
36 has its strengths and weaknesses, but what they have in common is that the results are valid only within a space of scale and
37 time. This footprint is usually quite small, thus only a local scale could be represented by it. Recently, these methods were
38 extended to include remote sensing techniques for the regional and global scale (Leuning et al., 2008; Miralles et al., 2011,
39 2016; Anderson et al., 2008), but the quality of the output products possess still a potential for improvement (Pan et al.,
40 2020; Zeng et al., 2012). Among the operational measurements, the FLUXNET (<http://www.fluxnet.ornl.gov>) project has the
41 largest network with about 500 stations worldwide. The project allocates standardized eddy-covariance techniques since
42 1990s, and is still acting as main driver in advancing evaporation research (Mauder et al., 2018; Baldocchi et al., 2001; Jung
43 et al., 2011). Evaporation measurements are still scarcely available due to high costs and the problem of large-scale
44 representability (in comparison to e.g. discharge measurements).

45 Hence, mathematical modelling in favour of its feasibility is a practical substitute. Besides empirical formulas (Cerro et al.,
46 2021; Zeng et al., 2012; Feng et al., 2016), evaporation is often estimated by physically-based models (Liu et al., 2012;
47 Boulet et al., 2015; Beven et al., 2021; Mallick et al., 2018), in which Penman-Monteith (and Shuttleworth and Wallace
48 extension) formula is one of the most frequently used. This approach reduces potential evaporation to an actual one
49 accounting for the available water in the soil-plant system. Thus, it is incorporated into many land surface models and
50 frameworks regardless of scale: local, regional or even global (Zink et al., 2017; Leuning et al., 2008; Mallick et al., 2018).
51 Despite many efforts to improve evaporation models on different scales, large uncertainties still remain (Mueller et al., 2011;
52 Allen et al., 1998, p.56; Miralles et al., 2016, p.2). In general, the sources of uncertainties can be classified as following:
53 model structure and process representation, choice of an appropriate parameter set, meteorological input data, spatio-
54 temporal miss-scaling and evaporation measurements themselves (Mauder et al., 2018; Mallick et al., 2018; Mueller et al.,
55 2011; Zhang et al., 2010). Studying these sources of uncertainties from different approaches and frameworks gained more
56 attention in recent years, however most of these studies are limited by the focus on one single spatio-temporal scale (Liu et
57 al., 2012; Jung et al., 2011; Chang et al., 2018). Only a few researchers focused on clarifying the uncertainties in multiple
58 frameworks with multiple input datasets and simultaneously accounting for point, regional and global scales (Winter and
59 Eltahir, 2010; Pan et al., 2020).

60 Here we aim to extend the knowledge of uncertainty in evaporation modelling by analysing the output of soil-plant-
61 atmosphere physically-based lumped BROOK90 model, which we integrated into three different frameworks. These



62 frameworks use different sources of data for the model parameterisation and forcing which represent various spatial scales,
63 namely global, regional and local. By mixing these different datasets and validating the simulated evaporation with eddy-
64 covariance measurements, we analyse which aspect of the framework possesses more uncertainty. In this study, we focus on
65 its two potential sources – the parameter set or the meteorological input. Thus, the outcome aims to provide a better
66 understanding of the BROOK90 model as well as the results should show the directions to improve effectively evaporation
67 simulations.

68 **2 Data**

69 **2.1 Eddy-covariance measurements**

70 The evaluation of simulated evaporation was carried for five sites with various land covers and long-term eddy-covariance
71 measurements (Fig. 1, Table 1). All selected towers are located in Saxony, Germany. The study area is characterized by
72 temperate suboceanic/subcontinental climate (Cfb, (Kottek et al., 2006)). The average temperature varies between $-15\text{ }^{\circ}\text{C}$ and
73 $+15\text{ }^{\circ}\text{C}$ in summer months and between $-5\text{ }^{\circ}\text{C}$ and $+5\text{ }^{\circ}\text{C}$ in winter months. The average annual precipitation varies between
74 750 mm and 960 mm. The measurements of atmospheric fluxes with standardized methods are operated by Technische
75 Universität Dresden within ICOS and FLUXNET projects. In this study, we used daily evaporation values calculated from
76 measured latent heat fluxes corrected for the observed site-specific energy budget closure gap. In general, from 10 (Hetzdorf)
77 up to 23 (Tharandt) years of continuous time-series are available.

78 The Grillenburg site (DE-Gri, the sensor height is 3 m above the ground) is a permanent and extensively managed (one to
79 three cuts per year) flat-terrain grassland (mesophytic hay meadow). Regular mowing usually takes place in June and
80 September. In the case of three cuts per year, the second one is usually done in July. Typical plant species include couch
81 grass, meadow foxtail, yarrow, common sorrel and white clover. The area is generally used for forage and rarely for pasture.
82 Vegetation height is measured once per week, with the lowest values (5-10 cm) measured at the beginning of growing season
83 or after cutting and highest values (typically 30-40 cm, maximum 90 cm) in the summer before cutting. Although the LAI
84 was only occasionally measured, the significant correlation between vegetation height and LAI made it possible to
85 interpolate the annual range. Therefore, the range of LAI was estimated between $0.25\text{ m}^2\text{ m}^{-2}$ and $5\text{ m}^2\text{ m}^{-2}$ in the yearly
86 course. The topography around the site promotes cold air deposition, thus daily minima of air temperature are often much
87 lower than at the other sites. The site is mainly characterized by gleysol soil that contains silty loam, loam, and loamy silt as
88 soil textures.

89 The Klingenberg site (DE-Kli, the sensor height is 3.5 m above the ground) is an intensively farmed arable land located 4 km
90 south from the Tharandt forest (Fig. 1). This site is characterized by annual and inter-annual crop rotation of rapeseed
91 (*Brassica napus*), winter wheat (*Triticum aestivum*), forage maize (*Zea mays*), spring barley (*Hordeum vulgare*) and winter



92 barley (*Hordeum vulgare*) with occasional intercropping. As a result, plant cover, vegetation height, LAI and rooting depth
93 varied greatly across time periods, i.e. measured annual maximum canopy height values vary between 0.7 m and 2.2 m and
94 LAI could reach up to 6 m² m⁻². Soil properties and runoff behaviour are strongly influenced by tillage and fertilizer
95 application. According to the (Ad-hoc-AG Boden, 2005), the soil was classified as gleysol and has a clay or loam texture.

96 The Hetzdorf site (DE-Hzd, the sensor height is 5 m (2010-2017), 11.5 m (2017-2021) and 17.5 m (since 2021) above the
97 ground) is a young oak (*Quercus robur*) forest planted after the Kyrill storm in 2007, which caused severe windthrow (40 ha)
98 in an old Norway spruce (*Picea abies*) forest. This site has a moderate slope to the North and a main wind direction to the
99 South due to a gap in the surrounding old spruce forest. The young oak stand is approximately 8-10 m high (2021) and
100 enclosed by spruce forest (up to 30 m height). Due to the high amount of deadwood and the young oak plantation until 2017
101 this ecosystem was a net CO₂ source, but since 2018 it already acts as a moderate CO₂ sink. As a young growing site, LAI
102 varies dynamically from year to year and was only measured sporadically. The site is dominated by pseudogley soil with a
103 silt and silty loam texture.

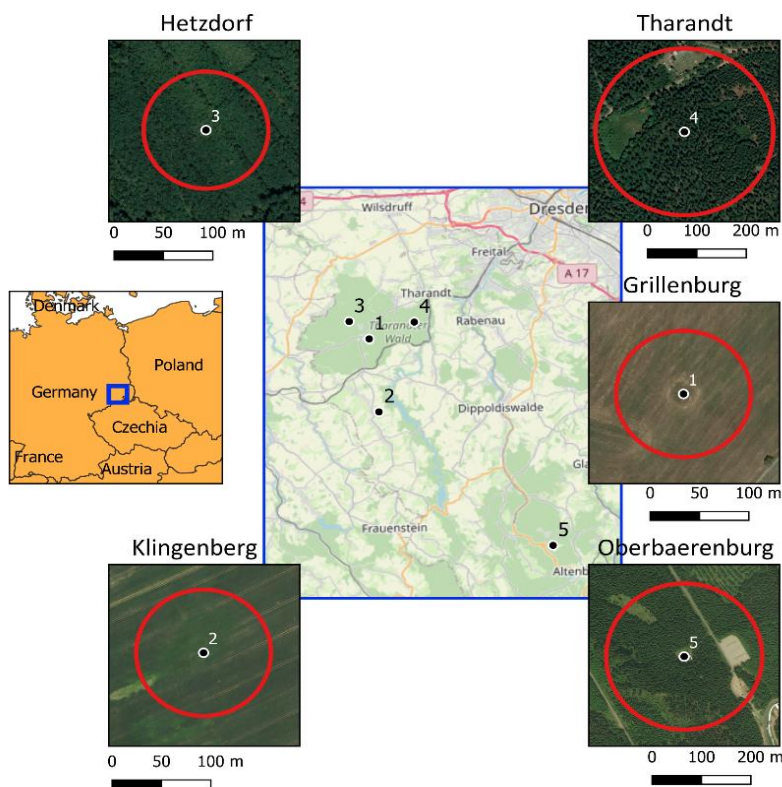
104 The Tharandt site (DE-Tha, the sensor height is 42 m above the ground) is a 120-year-old mixed conifer forest with a mean
105 canopy height of 30 m, consisting mainly of Norway Spruce (*Picea abies*, 80 %), European larch (*Larix decidua*, 18%), and
106 various other evergreen and deciduous tree species (2 %) such as Scots pine (*Pinus sylvestris*), Silver birch (*Betula pendula*)
107 and Mountain ash. Root depth amounted between 30 cm and 40 cm, relative to the predominant Spruce tree. The forest was
108 thinned five times (1983, 1988, 2002, 2011 and 2016) and European beech (*Fagus sylvatica*) and Silver fir were planted in
109 the understorey in 1995 and 2017, respectively. The site has silty podzol soils with relatively high stone content (10-20 %).
110 These soils were developed from a periglacial sediment consisting of debris from rhyolite and loess and are very
111 heterogeneous.

112 The Oberbaerenburg site (DE-Obe, the sensor height is 30 m above the ground) is an 80-year-old dense evergreen forest 15-
113 17 m height with predominantly Norway spruce trees (*Picea abies*). In contrast to the other sites, this site is located much
114 higher (734 m a.s.l.) with a prevailing NW wind direction and mean temperature and precipitation of 6.90C and 960 mm,
115 respectively. Spruce density has been thinned over the years (e.g., 1057 trees ha⁻¹ in 1994, 987 trees/ha in 2000, 884 trees ha⁻¹
116 in 2005, and 846 trees ha⁻¹ in 2011). However, this has had little effect on the site characteristics. The soil is characterized
117 as podzol and has a sandy texture with high stone content (20-40 %).

118 Due to the principles of eddy-covariance measurements, the observed fluxes refer to a certain footprint that varies depending
119 on wind speed, wind direction and atmospheric stability. Moreover, it is also affected by the height of measurement and the
120 surface roughness. According to long-term micro-meteorological measurements around the study sites, it was found that in
121 relation to predominant weather conditions the area of the highest flux density of the eddy-covariance signal (90 %) was
122 within a radius of 120-380 m. The values differ significantly among sites, but not greatly between wind directions (< 10 %).



123 Thus, equidistance footprints for each station (red circles on Fig. 1, shape files can be found in Supplementary) were
 124 assigned as mean values from all wind directions. These values are further used in the simulations in model frameworks.
 125 Selected daily evaporation data and other climatological variables can be found in the Supplementary.



126

127 **Figure 1. Location of chosen FLUXNET sites. Red circles represent footprints for each tower. OpenStreet Maps (© OpenStreetMap**
 128 **contributors 2021. Distributed under the Open Data Commons Open Database License (ODbL) v1.0.) and Bing Satellite images (©**
 129 **Microsoft) are used as a background.**

130

Table 1. Short summary on the chosen FLUXNET sites.

ID	Site name	Latitude	Longitude	Available data	Footprint, m	Dominant soil type	Land cover type
1	Grillenburg	50.950	13.513	2003-2020	135	gleysol	Permanent grassland
2	Klingenberg	50.893	13.522	2005-2020	135	gleysol	Agriculture (with crop rotation)
3	Hetzdorf	50.9641	13.490	2010-2020	125	pseudogley	Young oak forest (after storm)
4	Tharandt	50.963	13.565	1997-2020	360	podzol	Old spruce forest
5	Oberbaerenburg	50.787	13.721	2008-2020	350	podzol	Spruce forest



131 2.2 Climate data

132 We have chosen ERA5 (Copernicus Climate Change Service (C3S): ERA5: Fifth generation of ECMWF atmospheric
133 reanalyses of the global climate. ERA5 hourly data on single levels from 1979 to present., 2020), RaKliDa (Kronenberg and
134 Bernhofer, 2015) and in-situ station measurements to represent the global, regional, and local scales, respectively, as
135 meteorological forcing for the BROOK90 frameworks (see Sect. 3.1). The list of standard climatological variables required
136 to run BROOK90 consists of minimum and maximum 2 m air temperature, mean 10 m wind speed, solar radiation on the
137 horizontal surface, vapour pressure, and precipitation. Typically, daily data is required; however, if available, sub-daily
138 precipitation data is more favourable.

139 The ERA5 is a global climate reanalysis dataset from Copernicus and European Centre for Medium-Range Weather
140 Forecasts, available from 1950 to near real time at hourly resolution. It was derived using data assimilation principles by
141 combining a global physical model of the atmosphere and observations from around the world. The original model resolution
142 is 0.28125°, which corresponds to about 31*20 km rectangle in the area of interest. For the present study, data from the
143 nearest to each site ERA5 grid was downloaded and processed by aggregating hourly to daily values.

144 RaKliDa is an open-source daily climatological dataset covering the south-eastern part of Germany (namely Saxony,
145 Saxony-Anhalt and Thuringia) with a time span of 1961-2020. The original station data from the German Meteorological
146 Service and the Czech Hydrological Meteorological Institute are first corrected for wind errors (Richter, 1995) and then
147 interpolated on a 1x1 km grid using the Kriging indicator (Wackernagel, 2003). This approach is intended to reflect the
148 orographic influence of downwind and upwind effects and to account for convective and small-scale precipitation events. As
149 with ERA5, the nearest grid to each tower grid was used.

150 Daily meteorological data was taken from standard climate stations located in close proximity to the eddy-covariance towers.
151 Exception is the wind speed, which is measured on the same height with eddy-covariance. In addition, the available net
152 radiation was assimilated above the canopy. Prior data analysis revealed up to 15 % of missing values (depending on
153 location and variables). Since these values are generally not drastic, the majority of the missing parts fall within the model
154 “warm-up” period, and the variance of the most problematic variable (wind speed) within a site is not very high; it was
155 decided to fill the gaps with simple monthly averages.

156 All of the inputs required by BROOK90 are directly available in all three data sets, except for the vapour pressure, which
157 was calculated using dew temperature data (Murray, 1967) for ERA5 and mean daily temperature with relative humidity for
158 two others (Magnus formula).

159 The meteorological data prepared for BROOK90 can be found in Supplementary. A graphical overview of the differences
160 between three data sets is presented in Appendix A and will be discussed later on.



161 **3 Methods**

162 **3.1. BROOK90 setups**

163 In the study, four different BROOK90 setups are used to simulate evaporation and its components, with the BROOK90
164 model as the main core: Global BROOK90, EXTRUSO, BROOK90 with manual parameterization and calibrated
165 BROOK90.

166 BROOK90 (BROOK 90: A simulation model for evaporation, soil water, and streamflow., 2021) is a 1D process-oriented
167 model for simulation of vertical water fluxes in soil-plant-atmosphere systems. Precipitation input (snow or rain) first goes
168 through the canopy, where it could be intercepted and then evaporated. The portion, which reaches ground level, could be
169 infiltrated, frozen, evaporated, converted to surface flow, percolated or stored as soil moisture. Infiltrated water follows a
170 top-down approach as a macropore bypass and matrix flow. The soil column has groundwater, seepage and downslope
171 outflow. Finally, soil water storage is used for evaporation and transpiration. The model has more than 100 physically-based
172 input parameters, but typically most are straightforward and can be set easily (as location or slope). As the study mainly
173 reflects evaporation, this part of the model is described in more detail.

174 The model uses a two-layer version of Penman-Monteith (PM) equation by Shuttleworth-Wallace (SW) (Shuttleworth and
175 Wallace, 1985) to estimate the potential evaporation (PE) separately for canopy and soil surface accounting for the surface
176 energy budget and the gradient for the sensible heat flux respectively. Canopy-dependent PE consists of evaporation of
177 intercepted snow and rain and plant transpiration. It is defined as the maximum evaporation that would occur from a given
178 land surface under given weather conditions if all plant and soil surfaces were externally wetted. Surface-dependent PE
179 includes evaporation from soil and snow surfaces. It is defined as the maximum evaporation that would occur from a given
180 land surface under given weather conditions if plant surfaces were externally dry and soil water was at field capacity. The
181 SW method considers multiple resistances like the above canopy, within canopy from canopy and ground, canopy surface,
182 vapour movement in soil. They are applied in the standard PM equation, thus giving separate estimates of all five
183 components of PE. It should be noticed, as BROOK90 distinguishes between soil and plant evaporation, only one canopy
184 process and one ground process can occur at a given timestep. Subsequently, actual evaporation (E) is based on the water
185 availability in the system (within the canopy, on the soil and within the soil matrix). Daily evaporation rates are calculated as
186 a weighted sum of the daytime and nighttime values (based on the sunshine duration); however, interception could be
187 estimated at a higher frequency (hourly).

188 Originally, the model was written in FORTRAN programming language, here we used an R ‘line-by-line’ direct translated
189 version (BROOK90 in R, 2020).



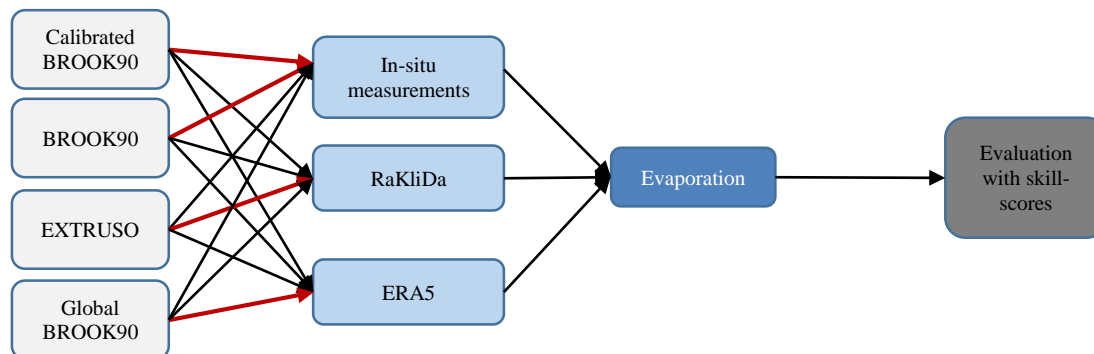
190 The Global BROOK90 (GBR90) framework incorporates open-source global datasets for parameterization and forcing of the
191 model using an R-package. The main feature of the package is wrapping of the modelling process in a fully automatic mode
192 based only on the location and time-interval input. The package uses global datasets for elevation (Amazon Web Service
193 Terrain Tiles), land cover (Land Cover 100 m), vegetation (MODIS) and soil characteristics (SoilGrids250), and
194 meteorological forcing (ERA5 reanalysis). The input area of interest is divided in a regular 50*50 m grid, and then hydro
195 response units (HRU) are identified based on the unique combinations of land cover (23 classes with fixed parameters), soil
196 characteristics (11 classes of soil texture used to assign fixed soil hydraulic properties; soil depth to the bedrock and fracture
197 of coarse fragments), and topography (aspect and slope). The model is then applied separately to each HRU and an area-
198 weighted mean is calculated. A more detailed description of the framework is presented in (Vorobevskii et al., 2020).

199 The EXTRUSO (EXTR) is similar to the GBR90 setup and is distributed via R-package, but operates with CORINE for land
200 cover, BodenKarte50 for soil type and Open Sensor Web for meteorological data. These datasets have higher resolution and
201 quality, but make the framework applicable only on a regional level (up to now only in Saxony, Germany). The HRU subset
202 in EXTRUSO is based on the overlay of soil and land cover data, however due to specifics of the datasets (polygons rather
203 than regular grid rasters) HRUs do not have fixed dimensions. The framework has fixed parameterization for 5 land cover
204 types (which are more general than the original types in CORINE) and 11 soil types (as in GBR90 based on soil texture
205 class). The 10 m digital elevation model is used for slope and aspect estimates. As in GBR90, BROOK90 is run for each
206 HRU and an area-weighted mean is stored. A full description of the framework is available at (Luong et al., 2020).

207 Finally, we made a setup using the original BROOK90 model (BR90) with manual parameterization based on long-term
208 field measurements (for canopy, i.e. height, LAI, conductivity), soil profile data (soil texture, depth, stone fracture) and
209 expert knowledge. Furthermore, we also calibrated BROOK90 for each site with in-situ meteorological data. This setup
210 (CBR90) serves as a benchmark for all other runs (more in detail in Sect. 3.3).

211 **3.2. Evaluation of parameterization and forcings combinations**

212 To assess the uncertainty of the BROOK90 setups with regard to the evaporation components, we propose to create different
213 combinations of the framework's parameterizations from global, regional and, local schemes and meteorological inputs from
214 global, regional and local datasets (Fig. 2). Additionally, we tested the sensitivity of the setups to the temporal resolution of
215 the forcing data (hourly and daily for ERA5). Our main hypothesis is that the goodness of fit of the setups decreases from
216 global to local scale (for both parameterization and forcing). We were particularly interested in testing the local-global
217 combinations, i.e. BROOK90 with ERA5 forcing and Global BROOK90 with station data forcing.



218

219

220

Figure 2. Principal scheme of the framework's mixture. Red arrows represent the original “parameter set – meteorological forcing” combination.

221

222

223

224

225

226

From the model runs, we extracted total evaporation and its five components: transpiration, evaporation of intercepted snow and rain, evaporation from soil, and snow evaporation. These results were evaluated on daily and monthly scales for the whole year and separately for the winter and vegetation periods using the following performance metrics: Mean Absolute Error, Nash-Sutcliffe Efficiency (NSE) (Nash and Sutcliffe, 1970a) and Kling-Gupta Efficiency (KGE) (Gupta et al., 2009a). The last one can be decomposed into three main components important to assess process dynamics: correlation, bias, and variability errors. Since all the proposed metrics are well known, we omit formulas in main text and list them in Appendix B.

227

228

229

230

Additionally, to test the uncertainty of the obtained performance, a small data resampling experiment was designed (here only for the daily KGE values). Thus, for each station we calculated multiple KGE values with reduced time-series length by randomly (1000 samples with replacement) throwing away 3 years of data (same for all cross-combinations). Obtained values serve to assess the possible KGE spread for each framework and meteorological dataset.

231

3.3. Setting the benchmark – the BROOK90 calibration

232

233

234

235

For the calibration of BROOK90, we choose a multi-objective optimizer recently developed for the calibration of hydrological models. The algorithm is a hybrid of the MEAS algorithm (Efstratiadis and Koutsoyiannis, 2005), which uses the method of directional search based on the simplexes of the objective space and the epsilon-NSGA-II algorithm with the method of classification of the parameter vectors archiving management by epsilon-dominance (Reed and Devireddy, 2004).

236

237

238

239

240

241

Here, we performed calibration and validation with a 70 % – 30 % data split focusing on maximising daily KGE values for total evaporation for the growing season (March-October) and the winter period (November-February). The initial parameter sets were set by “expert-knowledge”. Calibration within a physically meaningful parameters’ range was applied to the total 20 parameters. In general, these include albedo, vegetation and flow characteristics. Meteorological forcing was derived from in-situ measurements. The total number of trials was limited to 1000 model runs, which was sufficient to achieve stable performances for all three optimization functions.



242 Results of the calibration and validation are presented in Table 2. A complete list of chosen parameters with given ranges
243 and a graphical overview of the resulting Pareto fronts for each site are provided in Appendix C. The raw outputs of
244 calibration results for all trials with optimized parameters can be found in the Supplementary. It can be stated that calibration
245 and validation showed satisfactory results for the vegetation period even on a daily scale, while the results for the winter
246 time were poor at most sites (more in detail in Sect. 5.2 and 5.3).

247 **Table 2. Daily Kling-Gupta-Efficiency for BROOK90 calibration and validation.**

ID	Site name	KGE (Vegetation period)		KGE (Winter period)	
		Calibration	Validation	Calibration	Validation
1	Grillenburg	0.89	0.81	0.49	0.44
2	Klingenberg	0.72	0.67	0.19	-0.03
3	Hetzdorf	0.82	0.75	0.30	0.17
4	Tharandt	0.72	0.69	0.26	0.14
5	Oberbaerenburg	0.72	0.61	0.02	-0.94

248

249 4 Results

250 4.1. Daily and monthly total evaporation

251 Before discussing the performance criteria, a visual analysis of the modelled evaporation was performed. Therefore, daily
252 (for 2020) and monthly (for the whole period with available measurements) time-series (Appendix D), monthly quantile-
253 quantile (Fig. 3) and mean monthly (Fig. 4) plots were analysed.

254 Daily evaporation of 0-0.5 mm in winter and up to 6-7 mm in summer months (with a maximum of about 10 mm) was found
255 for the Grillenburg's grassland. All model setups showed similarly low values in November-February. The growing period
256 (March-May) was represented with a delay of 3-4 weeks for GBR90 and EXTR and 2-3 weeks for BR90. Calibration helped
257 to eliminate this time shift on a monthly scale, however at the same time enhancing the unreasonably high variability on a
258 daily scale. During the summer months (June-August), the frameworks suffered increasing variance and systematic
259 underestimation, which got worse with the higher values. Moreover, monthly maximum values vary from year to year due to
260 differences in the timing of grass cuts. Evaporation in autumn is well captured but advanced by 2-3 weeks in EXTR and
261 BR90. Finally, the difference between meteorological datasets is only noticeable in the summer months.

262 In Klingenberg's crop field, evaporation of 0-1 mm in winter and 4-6 mm in summer months (with maximum around 9 mm)
263 is usually observed. In most of the years, all model setups showed a similar small overestimation in November-January. It
264 was relatively difficult to achieve good timing for the vegetation period even on a monthly scale. Since the growing and



265 harvest periods of the various crops differ by up to two months and the annual rotation with clear cuts are irregular. The
266 growing period (February-May) had in general a delay of 2-6 weeks. Here CBR90 shows higher daily evaporation values,
267 thus fitting good BIAS, while the variation stays underestimated. In contrast with the grassland site, summer months (June-
268 August) did not depict a high bias, the main uncertainty lies in a considerable scattering, which is higher in the middle part of
269 QQ-plot. Furthermore, the different setups showed different peak values in the summer months, BR90 matched observations
270 in June, while GBR90 and EXTR showed the maximum in July. Finally, in autumn, none of the setups provided satisfactory
271 results, namely both over- and underestimations, especially in September and October. Again, based on the meteorological
272 datasets, the variability of the model performance is visible only in the summer months.

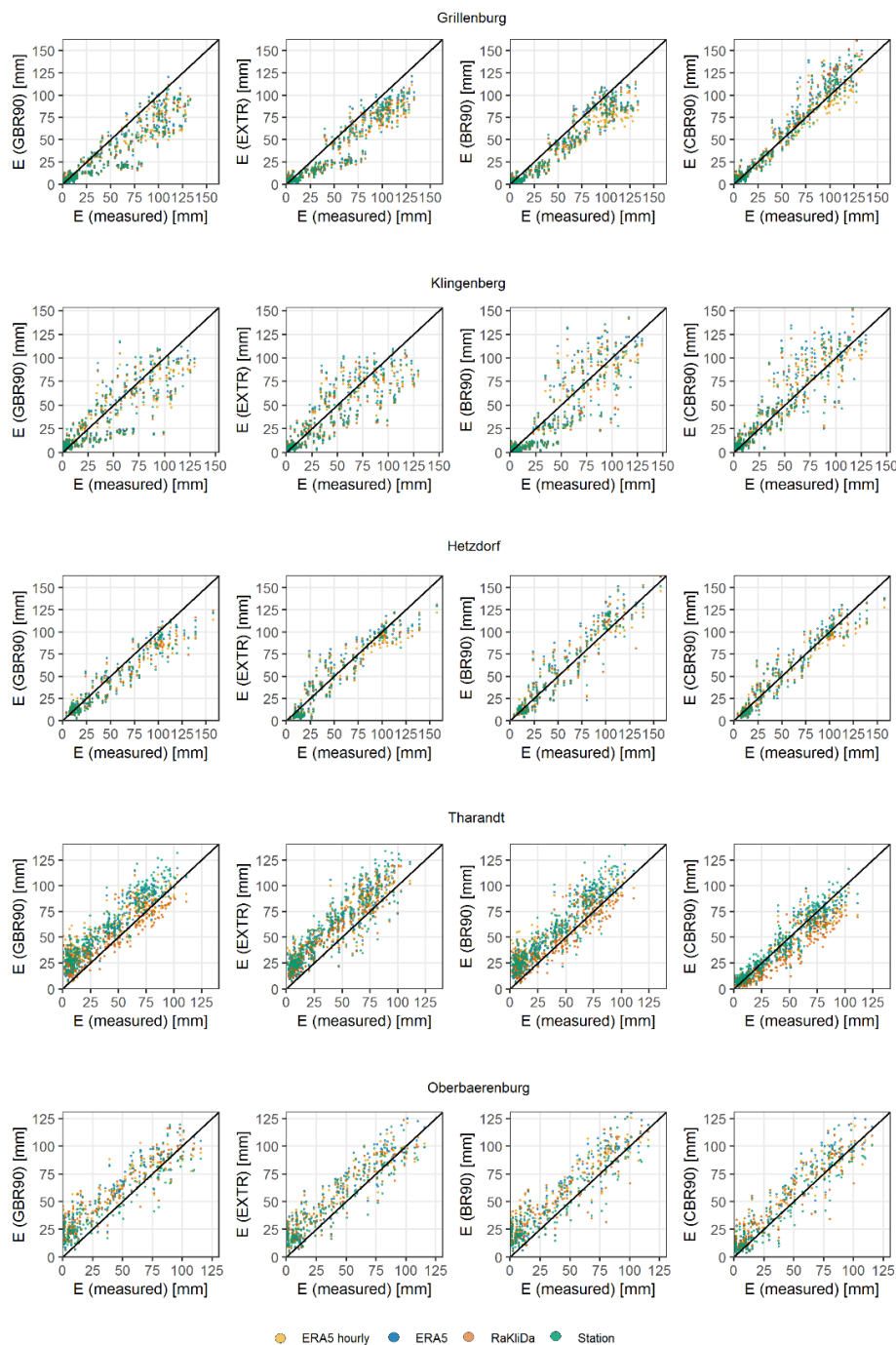
273 For the Hetzdorf deciduous broadleaf forest, typical values of winter and summer evaporation are 0-1 mm and 3-5 mm (with
274 maximum around 8.5 mm), respectively. All model setups showed small amounts of evaporation in winter with a low bias,
275 but also low correlation. The main leaf development period (March-May) was represented well by GBR90, with a 2-3
276 weeks' time lag in April for EXTR and BR90. In the summer months (mostly in June and July) GBR90 and EXTR
277 underestimated evaporation by 10 %, while 'expert knowledge' BR90 gave positive BIAS. It can be noticed on the monthly
278 plots that as the forest keeps developing and growing intensively within the last 10 years, higher evaporation rates were
279 observed from year to year. At the same time due to model parameter stationarity, BR90 shows closer to the observed
280 evaporation values only in the last two years. The annual mean monthly peak (July) and leaf fall were well captured by all
281 models. Here the variance errors reach minimum values in comparison to all the other sites. Only for the summer months, a
282 rather small difference of about 10 mm per month between the meteorological forces could be captured.

283 In the evergreen coniferous forest of Tharandt, daily evaporation usually yields 0-0.3 mm in winter and 2-3 mm in summer
284 (with maximum around 7 mm). All setups except CBR90 demonstrated a high BIAS for the seasons (15-20 mm per month),
285 which is larger in winter, where daily peaks are sometimes as high as summer maximums. Moreover, the inter-annual
286 variability appears to be highly overestimated as well. Like for the grassland, the model calibration reduced the mean error to
287 optimum values, but the problem of daily peaks in winter remained unsolved. In contrast to the other sites, a noticeable
288 difference between forcings can be observed (up to 10 % in the summer months) with the in-situ measurements delivering
289 the highest evaporation amount.

290 The evergreen coniferous forest of Oberbaerenburg normally has evaporation rates of 0-0.3 mm in winter and 2-3 mm in
291 summer (with maximum around 8 mm). Evaporation here is 5-10% higher in the growing season than at the Tharandt site.
292 Still, most of the setups (except in spring and CBR90) showed a positive BIAS, which is higher in winter and July. Similar
293 to Tharandt, winter daily peaks sometimes exceeded summer extremes. Here, even the calibrated model did not demonstrate
294 a good agreement in general and did not remove winter overestimations. Oberbaerenburg was the only site where the well-
295 known European drought of 2018 is clearly visible on a monthly scale. The data shows around 30 % less evaporation in
296 summer months due to depletion of the soil water and overall precipitation deficit. However, most of the model setups did

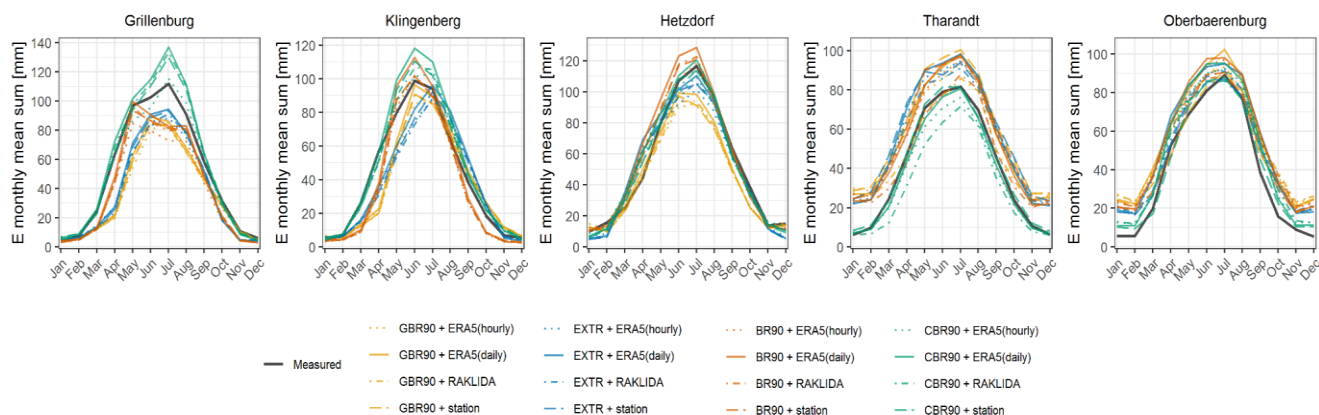


297 not depict this effect properly. Finally, the spread between meteorological datasets here is not as broad as for the Tharandt
 298 site.



299
 300

Figure 3. Observed and modelled monthly evaporation values for all setups.



301
302

Figure 4. Observed and modelled monthly mean evaporation values for all setups.

303 In Fig. 5, the daily KGE values are shown, while the monthly results and other criteria (NSE, MAE) are presented in
304 Appendix E. Based on KGE values, a good agreement was found between all model setups and observations for all the sites
305 (Fig. 5). The best agreement showed the combination “CBR90 + station data” (from 0.72 in Oberbaerenburg to 0.91 in
306 Grillenburg) and the worst “GBR90 + hourly ERA5” (from 0.36 in Grillenburg to 0.71 in Hetzdorf). On the monthly scale,
307 all setups demonstrated higher performance, which is approximately 5 % better than on the daily scale. The Goodness of fit
308 in the vegetation period was better and very similar to the whole year, while in winter all setups performed not so well,
309 resulting sometimes in negative KGE values (down to -0.6). Here BR90 and EXTR showed distinctly worse outcomes in the
310 fields (Grillenburg and Klingenberg) and in the deciduous forest (Hetzdorf) respectively.

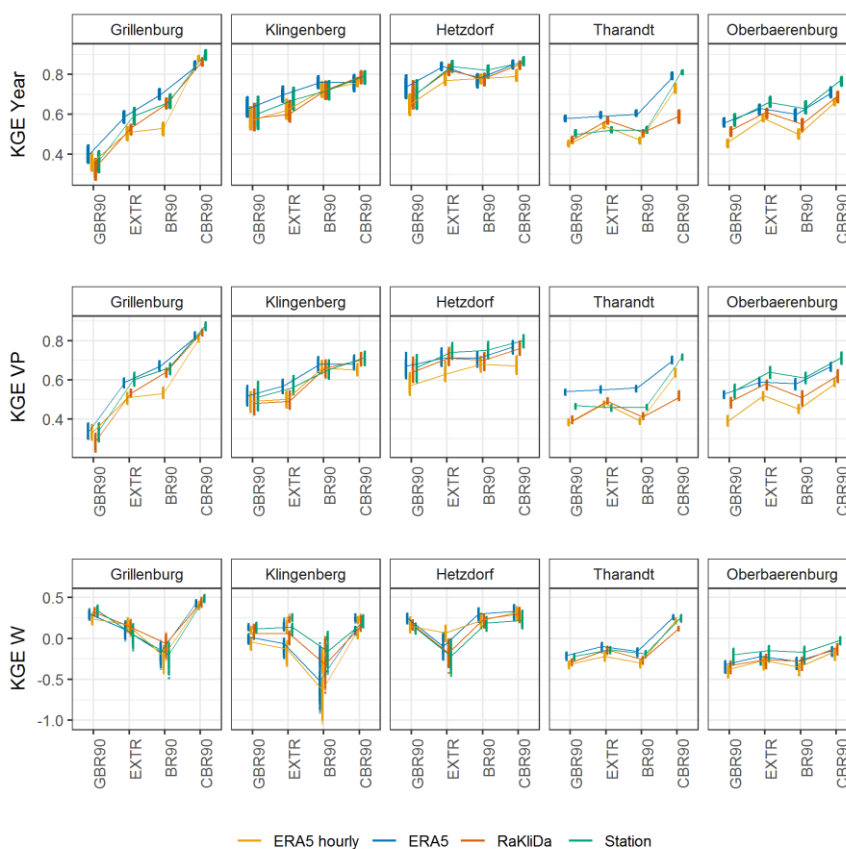
311 With a few exceptions, the best performance among the meteorological datasets was achieved for the station data and ERA5.
312 The hourly-resolved ERA5 data did not produce better results, showing the worst performance on the annual scale in most
313 cases. On average, in terms of KGE values, the spreads in the meteorological forcings yielded 0.1 (maximum of 0.17 showed
314 BR90 for Grillenburg), while scattering in the parameterization schemes was much higher and yielded 0.25 (with the
315 maximum of 0.5 for Grillenburg). These outcomes, coupled with the fact that CBR90 showed significantly higher
316 performance than other setups for almost all the sites, indirectly confirmed the higher sensibility of the BROOK90 model to
317 the parameterization scheme rather than to meteorological forcing. However, the calibration success was primarily due to
318 improvements in the vegetation period, while only minor changes occurred in winter (except for the Tharandt site). Anyway,
319 these conclusions need to be backed up with the assumption that both meteorological data and parameters used for each
320 spatial scale come from state-of-the-art sources. Thus, they are both representative and possess the best quality (currently)
321 for global, regional and local scales respectively.

322 Finally, KGE spreads calculated for each combination from a resampled time-series are generally small. On the annual scale
323 and for the vegetation period, higher uncertainties were found in Grillenburg, Klingenberg and Hetzdorf (10-15 % on



324 average); while in Tharandt and Oberbaerenburg KGE deviations were low (around 5 %). For the winter months, the spread
 325 possessed the same behaviour, but resulted in much higher values (up to 100%). Among all the frameworks, GBR90 was
 326 associated with the largest uncertainty on the annual scale in almost all the cases, while it had the smallest spread in the
 327 winter, where uncertainty of EXTR and BR90 dominated.

328 NSE values are in general similar to KGE, but slightly smaller, which range from -0.05 for GBR90 in Grillenburg and
 329 Oberbaerenburg to 0.88 for CBR90 with station data. Mean average errors vary from 0.39 up to 0.98 mm*day⁻¹ with the
 330 highest values in evergreen forests for GBR90 and the lowest in Grillenburg for CBR90.



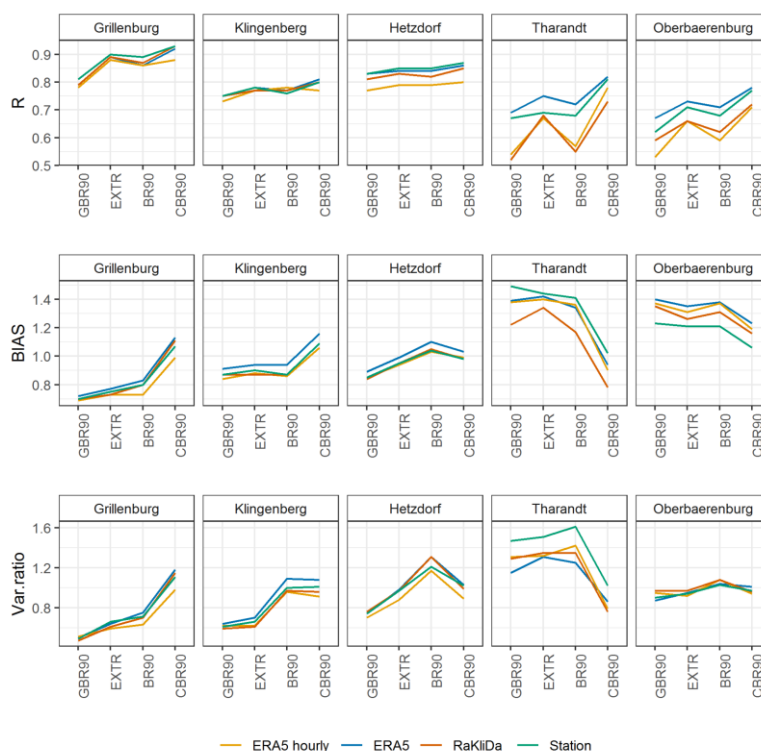
331

332 **Figure 5. KGE values for daily evaporation: whole year, vegetation and winter periods. Vertical lines for each cross-combination**
 333 **refer to bootstrapped KGEs.**

334 The major advantage of the KGE criteria is the possibility to obtain a deeper understanding of model uncertainty through its
 335 decomposition. A closer look at the KGE components (Fig. 6) reveals that correlation coefficients for the fields (Grillenburg
 336 and Klingenberg) and deciduous forest (Hetzdorf) are relatively high for all model setups (0.75-0.95), and the main problems
 337 occur in underestimation of the mean (0.7-0.8) and variability ratios (0.55-0.7) (except for BR90 in Hetzdorf). In general,



338 there are only small fluctuations between model forcings for these three sites. In evergreen forests, on the other hand, the
339 correlation showed much higher spread among both parameterizations and meteorological datasets (0.4-0.75). Furthermore,
340 bias and variability are, on the other side, overestimated (except variability in Oberbaerenburg), especially in Tharandt (up to
341 1.6). Overall, ERA5 and station data perform better than others in most of the cases do. The hourly ERA5 forcing did not
342 produce a noticeable difference in evaporation bias or variability, but reduced correlation in the forests (by 5-15 %). Finally,
343 it could be noticed that in comparison to the other setups, CBR90 bring bias and variance ratio almost to one, but did not
344 improve correlation for all the sites (i.e. Hetzdorf).



345

346

Figure 6. Decomposition of KGE for daily evaporation for the whole year: correlation, BIAS and variance ratio

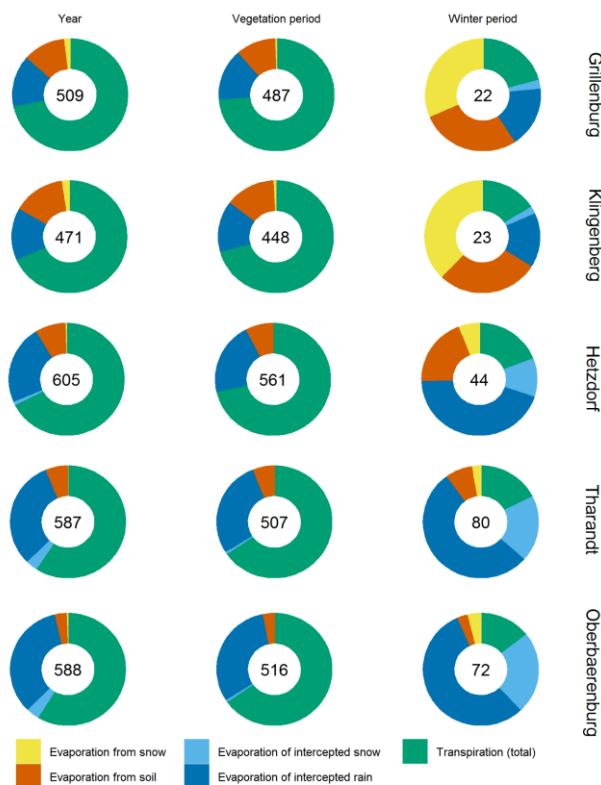
347 4.2. Evaporation components

348 The 40-60 % partitioning between total flow and evaporation components in global terrestrial water balance (Müller
349 Schmied et al., 2016) also applies to the BROOK90 point simulations. With a variation in mean annual precipitation from
350 877 mm (Klingenberg) to 1141 mm (Oberbaerenburg), measured mean annual evaporation varies from 476 mm (Tharandt)
351 up to 625 (Hetzdorf) mm. This leads to measured E-P ratios of 0.41 to 0.65, with the lowest values observed in old spruce
352 forest and the highest in grassland and growing deciduous forest. Here, both the global and regional frameworks showed an



353 overestimation of the ratio for the evergreen forests (Tharandt and Oberbaerenburg) and an underestimation for the fields
 354 (Grillenburg and Klingenberg) (could be found in Supplementary).

355 Overall, 60 % of annual global terrestrial evaporation consists of plant transpiration, 22 % of water attributes to evaporation
 356 from soil and snow and finally interception contributes up to 18 % (Wei et al., 2017). We summarized the annual
 357 evaporation component (Fig. 7) of all tested model setups. According to this figure, transpiration in fields and deciduous
 358 forest yields 68-73 %, and evergreen forest transpires about 58-59 %. In Tharandt and Oberbaerenburg 31-35 % of
 359 precipitation goes to interception (mainly rain, interception of snow is less than 2 %). In Grillenburg, Klingenberg and
 360 Hetzdorf evaporation of the intercepted precipitation is lower and yields 14-23 %. Soil evaporation on the other side, is
 361 higher in the fields (11-15 %) and lower in forests (4-8 %). Evaporation from snow is less than 2 % at all sites. The
 362 vegetation period spans 8 months in total and accounts for most of the annual evaporation (85-95 %). Thus, the distribution
 363 of components is generally consistent with a slightly higher contribution from transpiration. In winter, evaporation consists
 364 mainly of interception in forests and soil or snow evaporation of the fields.

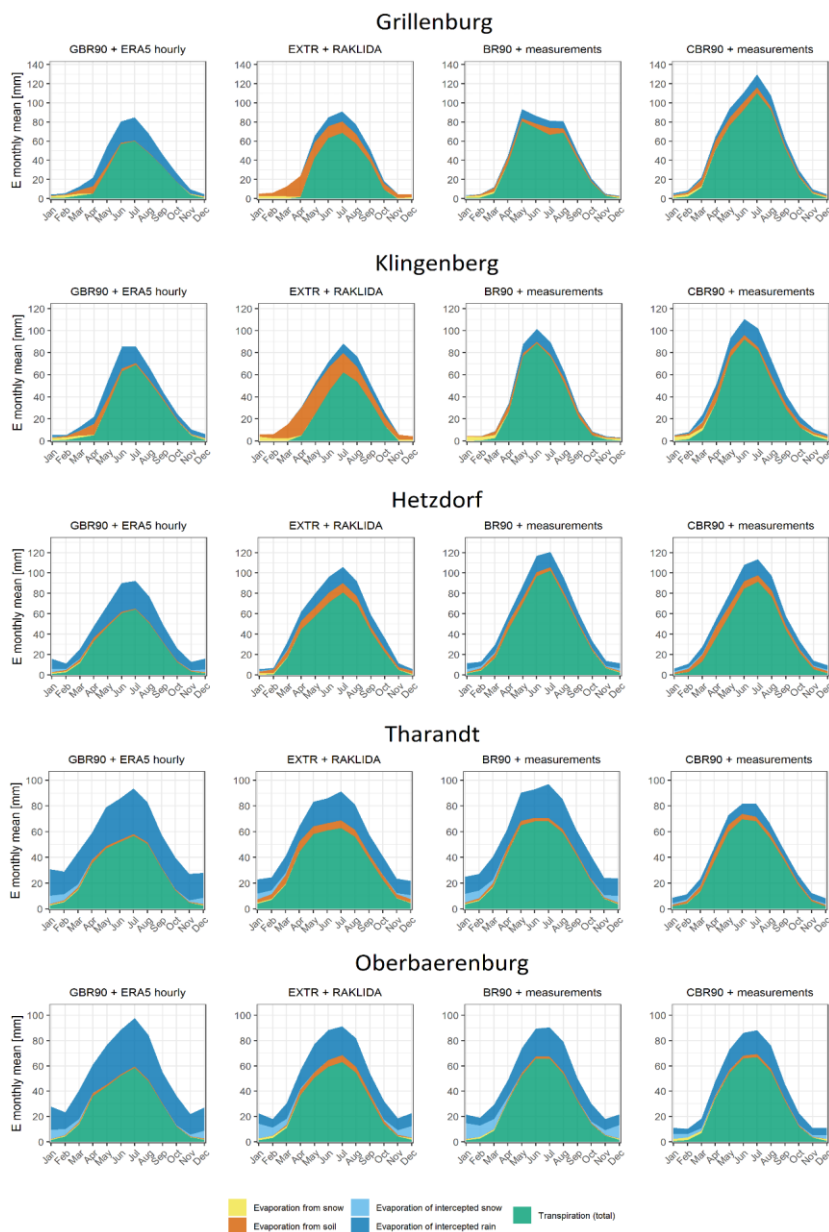


365

366 **Figure 7. Mean annual and seasonal evaporation components averaged over all model setups. The numbers inside pie charts refer**
 367 **to the mean evaporation sums per year or season.**



368 To get more insights on the possible setups' differences regarding the evaporation partitioning, we show “natural” model
369 parameterization and forcing combinations (Fig. 8). Only minor differences were observed in evergreen coniferous forests.
370 This mainly concerns intercepted rain. GBR90 with hourly ERA5 shows the largest amount (40-68 %) and CBR90 with
371 station data reduces interception up to 15-30 %, which is especially noticeable in Oberbaerenburg. At the other three sites,
372 seasonality plays a bigger role in the redistribution of evaporation components. Indeed, in the fields, almost no interception
373 was modelled in EXTR using RaKliDa and BR90 with station data in winter and early spring, and all evaporation in these
374 months consists of snow and soil evaporation. Furthermore, the transpiration is dominant in summer and autumn times with
375 sharper edges due to crop and grass cutting. In general, EXTR delivers more soil evaporation than other model setups, while
376 GBR90 produces more rain interception. Slightly smoothed but similar results could be observed in the deciduous forest of
377 Hetzdorf. Since the actual distribution of the components is unknown, we can only assume that CBR with in-situ
378 meteorological data indicates conditions that are the closest to reality. Considering this, we can rank the goodness of the
379 framework in the evaporation representation in the following order (best to worst by similarity to CBR90): BR90, EXTR,
380 GBR90, which seems indeed logical.



381
382

Figure 8. Modelled mean monthly evaporation components.

383 5 Discussion

384 5.1. Uncertainty of meteorological input

385 The uncertainty of the global and regional datasets due to the grid size, as well as the lack of representability of the “point”
386 station data for the footprint of the FLUXNET tower, could play a significant role in the modelling process. Although the



387 results showed that the meteorological input generally plays a smaller role than parameterization, it is worth analysing its
388 possible uncertainty.

389 Of the six input meteorological variables, net solar radiation and precipitation have the biggest influence on evaporation.
390 Global radiation in the gridded datasets showed minor but systematic overestimation compared to measurements on the
391 mean daily scale (around $1 \text{ MJ}\cdot\text{m}^{-2}\cdot\text{day}^{-1}$ in winter and $2\text{-}3 \text{ MJ}\cdot\text{m}^{-2}\cdot\text{day}^{-1}$ in summer months). However, summer variations
392 (peaks and minimums) are underestimated probably due to cloud coverage problems in ERA5 and RaKliDa. Precipitation
393 showed a much larger and non-systematic difference between the three datasets. In general, higher mean daily precipitation
394 was measured from September to March in Grillenburg, Hetzdorf and Tharandt ($0.5\text{-}2 \text{ mm}\cdot\text{day}^{-1}$). However, when looking
395 at the BIAS values (Table 3), a negative BIAS is typical for both datasets (except Klingenberg for both and Tharandt for
396 RaKliDa). The behaviour of the vegetation and winter periods separately follows the annual BIAS. Temperature and
397 available vapour pressure appear to be consistent, with 1-3 degree and 0.01-0.03 kPa respectively variation from
398 measurements in the summer months. The exception is Oberbaerenburg, where the maximum temperature and available
399 vapour pressure from ERA5 and RaKliDa have higher uncertainty, probably due to neglecting higher altitude in the datasets.
400 Finally, wind speed possesses a systematic positive bias ($1\text{-}2 \text{ m}\cdot\text{s}^{-1}$) for all months, except for ERA5 in forests and
401 Klingenberg.

402 Table 3. Precipitation BIAS (to in-situ measurements).

Site name	Meteo Dataset	Year	Vegetation period	Winter period
Grillenburg	ERA5	0.91	0.95	0.83
Klingenberg		1.05	1.05	1.05
Hetzdorf		0.92	0.96	0.85
Tharandt		0.96	1.01	0.85
Oberbaerenburg		0.76	0.85	0.59
Grillenburg	RaKliDa	0.88	0.92	0.8
Klingenberg		1.04	1.02	1.08
Hetzdorf		0.88	0.93	0.77
Tharandt		1.15	1.16	1.12
Oberbaerenburg		0.71	0.78	0.57

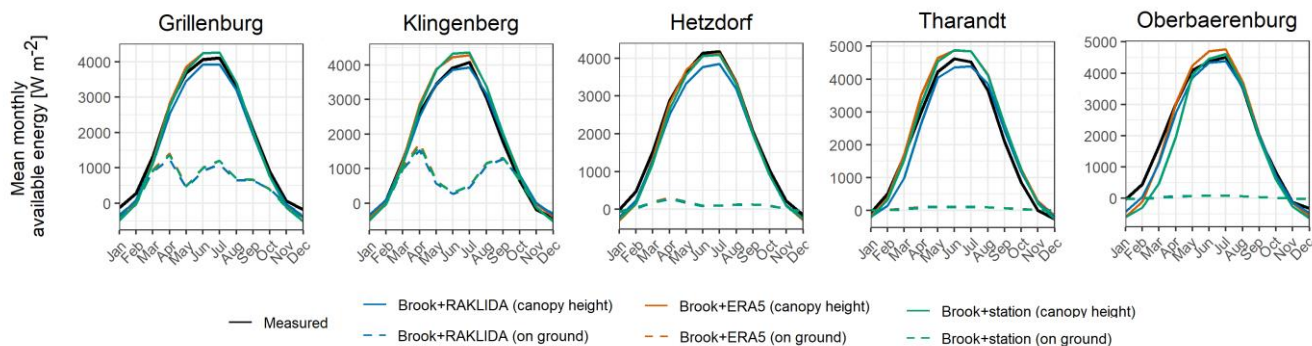
403 5.2. Challenges In the model process representation

404 Although BROOK90 has a fairly good physically-based description of the evaporation process, it shows some limitations as
405 well. For example, there is no allowance for non-green leaves, which intercept precipitation and radiation, but in the
406 meantime do not transpire. This process can play a role in deciduous forests like Hetzdorf in autumn and winter, as they
407 generate too much transpiration. Furthermore, since the phenomenon of ground frost is not considered, soil evaporation is



408 not limited on these days, which could lead to a substantial overestimation in winter. As canopy parameters are assumed
 409 constants, phenology or growth (e.g. crop rotation in Klingenberg and continuous forest growth in Hetzdorf) as well as
 410 drought affecting LAI (reduction due to prolonged water stress) are not considered in the model. Snowpack energy and
 411 evaporation modules suffer from overestimations in tall canopies, thus an arbitrary reduction factor is applied. Finally,
 412 albedo does not depend on solar elevation, canopy structure, or snow age. These limitations alone could have a substantial
 413 influence on total evaporation and its timing.

414 In addition, the PM equation uses vapour pressure deficit and net energy as the main factors to calculate potential
 415 evaporation. The first variable is derived directly from the daily input temperature and available vapour pressure using the
 416 Magnus equation and does not vary much between different methods (Lide, 2005). For net energy, the situation is different.
 417 The shortwave radiation is an input and its net value is controlled by the rather vague albedo, while the longwave radiation is
 418 estimated internally using the effective emissivity of the clear sky. Under these assumptions, the potential uncertainty
 419 between different formulas can be as high as 20-30 $W \cdot m^{-2}$. After obtaining a persistent positive BIAS in the forests, we
 420 checked the energy balance of the model with in-situ measurements (Fig. 9). In fact, minor differences were found for all
 421 input datasets. In the summer period, minor overestimation was found for ERA5 and station data in Grillenburg, Klingenberg
 422 and Tharandt, and underestimates for RaKliDa in Hetzdorf and Tharandt. In winter (especially in December and January),
 423 large relative underestimation was discovered in Grillenburg, Hetzdorf and Oberbaerenburg. Therefore, with a negative
 424 amount of energy, BROOK90 still showed higher monthly evaporation than measured. Specifically, according to Fig. 8, 90
 425 % of the actual evaporation in forests in winter consists of interception, and normally there is no absence of precipitation
 426 input during this period. Because of the peculiarities of the PM approach, positive potential evaporation can be estimated
 427 with negative net energy, positive vapour pressure deficit, and low estimated atmospheric and canopy resistances. Thus, as
 428 long as vapour pressure deficit exists, the evaporation flux tries to fill the gradient.



429
 430

Figure 9. Observed and modelled monthly mean net energy on canopy and ground level.



431 **5.3. Reliability of eddy-covariance measurements**

432 Largest systematic deviations between observed and modelled evaporation, which could be discussed in the context of
433 inaccuracy of the measurements, were discovered in the evergreen forests in winter, in grassland in summer and in pasture in
434 growing season. Therefore, we calculated grass-reference evaporation using the original FAO method and ran BROOK90
435 simulations (replacing original site-specific vegetation parameters with “grassland” ones from Grillenburg manual
436 parameterization scheme) using station meteorological data (Fig. 10).

437 The FAO approach showed very close values for all the sites except for Tharandt where for the vegetation period
438 evaporation was 20 mm higher. BROOK90 simulations, on the other hand, depicted higher variability between sites,
439 especially in the vegetation period (15-25 mm).

440 FAO simulations of field sites (Grillenburg and Klingenberg) fit with the observed data quite well, while BROOK90 showed
441 time lag and underestimation of evaporation in summer months. The time lag during the growing and harvesting periods for
442 Klingenberg could be explained with permanent crop rotation and inability of FAO and BROOK90 models to cope with non-
443 stationarity in vegetation parameters. Overestimation in winter for the FAO method for both sites could be a result of
444 simplifications of FAO-modified PM equation against SW approach in BROOK90 (i.e. neglecting the soil water holding
445 capacity). According to the continuous long-term measurements of grass height in Grillenburg, regular grass cutting is
446 performed in June-July. This in general should lead to evaporation decline, which can be seen clearly on Fig. 4 for monthly
447 evaporation of BR90. However, this effect was not found in the measurements (even on a daily scale). Moreover, mean
448 evaporation usually shows maximum annual values in July. Besides possible systematic measurement errors, this could be
449 explained either by an underestimation of the real site footprint or by permanent. Another explanation is near-saturation
450 conditions of the soils. Thus, almost unlimited water supply and perturbation of the evaporation components after grass
451 cutting (drastic increase of soil evaporation). Nevertheless, while calibrating the model, it was realized that it is impossible to
452 increase soil evaporation by almost 30 mm during the summer months and stay within the physically meaningful boundaries
453 for soil parameters for the given soil profile.

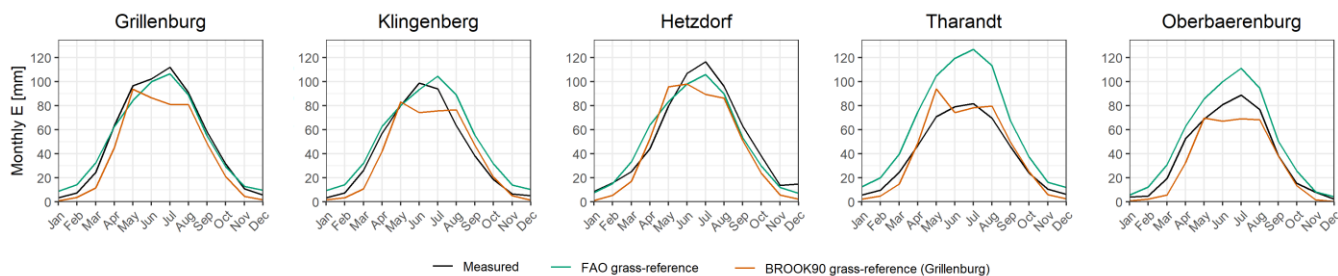
454 In Tharandt and Oberbaerenburg FAO evaporations are higher than the measurements, especially in summer months, while
455 BROOK90 gave similar values for Tharandt and lower for Oberbaerenburg. In winter months, FAO approach showed 10-20
456 mm, while BROOK90 resulted in 3-5 mm (consisting only of soil and snow evaporation). At the same time, all model setups
457 showed 20-30 mm of evaporation per month in winter (which is more than 80 % consists of intercepted precipitation), while
458 only 5-10 mm is observed. Thus, it is possible that the interception is generally underestimated by eddy-covariance
459 measurements in the forests. Moreover, while the calibration in Tharandt helped to adjust the simulated evaporation in
460 winter months as well (primarily by increasing the winter albedo), in Oberbaerenburg even a relatively wide parameters'
461 range was not sufficient. Here, the large variations between two approaches emphasize the importance of the soil and in a



462 regulation of the evaporation, since different soil types appear at the grassland and evergreen forest sites (gleysols and
463 podzols respectively).

464 In addition, previous analysis of eddy-covariance data for some of the study sites showed, that the possible under and
465 overestimations in measurements could be as large as $\pm 8-11\%$ for Tharandt, $\pm 29-36\%$ for Grillenburg and $\pm 28-44\%$ for
466 Klingenberg (Spank et al., 2013).

467 Therefore, in addition to reliability of the mean net energy and precipitation (Sect. 5.1 and 5.2), it is possible that the quality
468 of the eddy-covariance data is questionable due to at least systematic underestimation of interception and non-representative
469 footprint.



470

471

Figure 10. Observed and modelled monthly mean grass-reference evaporation.

472 Conclusion and outlook

473 This study presents the qualitative analysis and discussion of the BROOK90 model uncertainties with regard to evaporation
474 simulations. We tried to answer the question whether the model is more sensitive to the parameter set or to the
475 meteorological input. We used three frameworks (Global BROOK90, EXTRUSO and BROOK90 with manual
476 parameterization) and three forcing datasets (ERA5, RaKliDa, in-situ measurements) representing the global, regional and
477 local scale, respectively. We made cross-combinations of them and model evaporation components for five locations in
478 Saxony, Germany, covered by long-term eddy-covariance measurements: grassland (Grillenburg), cropland (Klingenberg),
479 deciduous broadleaf forest (Hetzdorf) and two evergreen needleleaf forests (Tharandt, Oberbaerenburg).

480 Our results indicated that all setups perform well even on a daily scale, with KGE values ranging from 0.35-0.80. KGE
481 decomposition demonstrated that with high correlation coefficients in grassland, cropland and deciduous forest performance
482 was affected here mainly by BIAS and variance ratios, whereas in evergreen forest all three components varied greatly. The
483 highest and lowest values among all setups were achieved by the same combination of Global BROOK90 and ERA5 in
484 Hetzdorf and Grillenburg respectively. Calibration of the model helped to increase KGE significantly, especially for



485 Grillenburg and Tharandt. The vegetation period where 90-95 % of the total annual evaporation is observed, showed much
486 higher agreement with the observations than winter period.

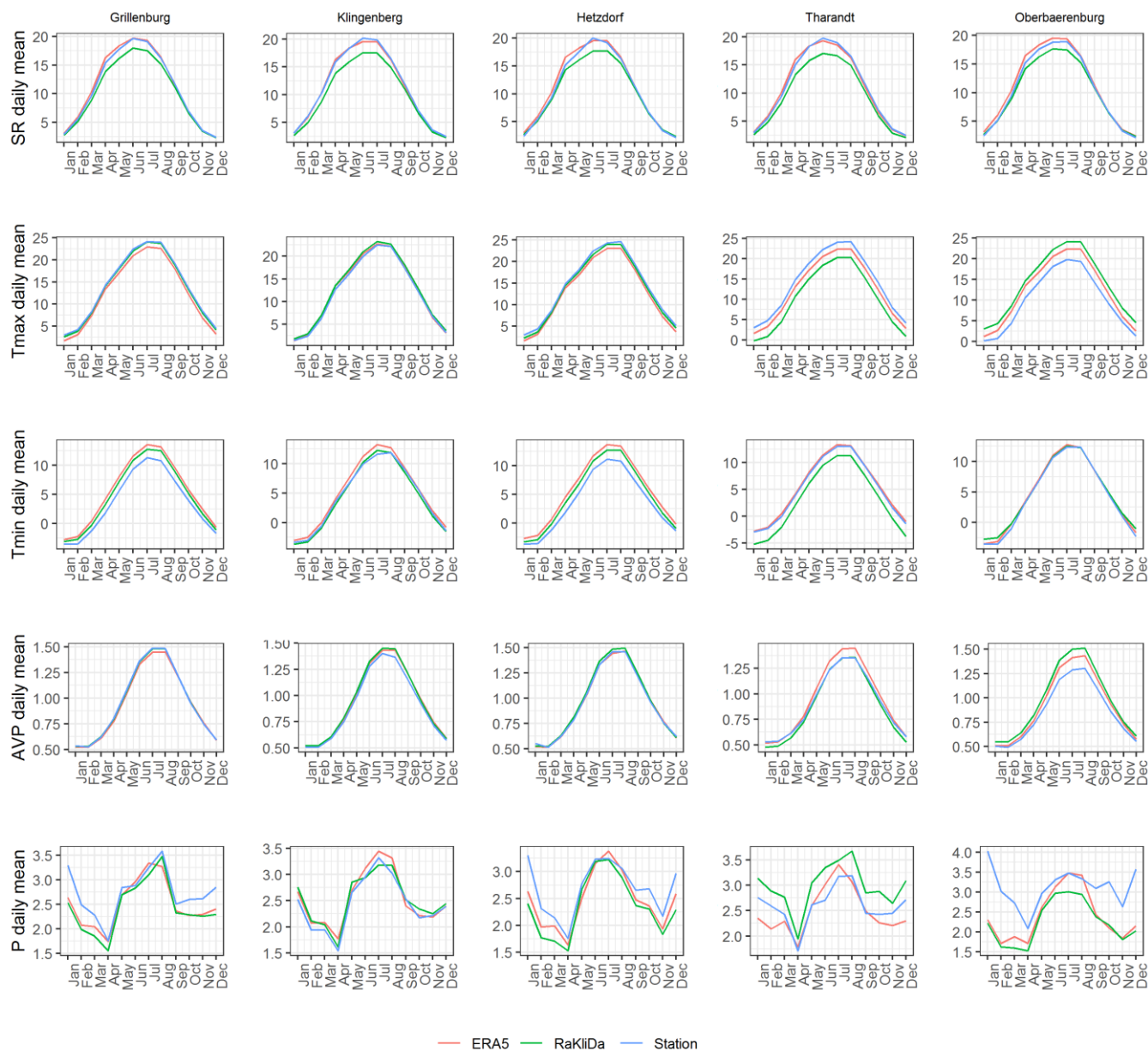
487 The main finding of the study is that for all tested setups, parameterisation gave us higher spread in model performance than
488 meteorological forcings for fields and evergreen forests sites. The opposite was observed in young deciduous forest. While
489 the difference in parameter sets mattered throughout the year, the difference in the meteorological datasets was evident only
490 in summer months. Analysis of the breakdown of evaporation components revealed that in the vegetation period
491 transpiration yields up to 65-75 % of total evaporation, while in the winter months interception (in forests) and soil/snow
492 evaporation (in fields) play a major role. Moreover, different parameter sets show substantial differences in the redistribution
493 of evaporation components. Finally, the discussion raised the questions of meteorological data quality, limitations of the
494 model and reliability of the eddy-covariance measurements.

495 In the outlook, we would like to suggest possible future directions on this topic:

- 496 • expand the number of study sites with other FLUXNET towers
- 497 • run similar analysis for other physically-based models
- 498 • analyse model uncertainty by incorporating runoff and soil moisture in the analysis
- 499 • apply and validate different methods to breakdown eddy-covariance data in components



500 **Appendix A. Comparison of BROOK90 meteorological input data (ERA5, RaKliDa and station measurements)**



501
 502

Figure A1 Monthly daily mean meteorological variables

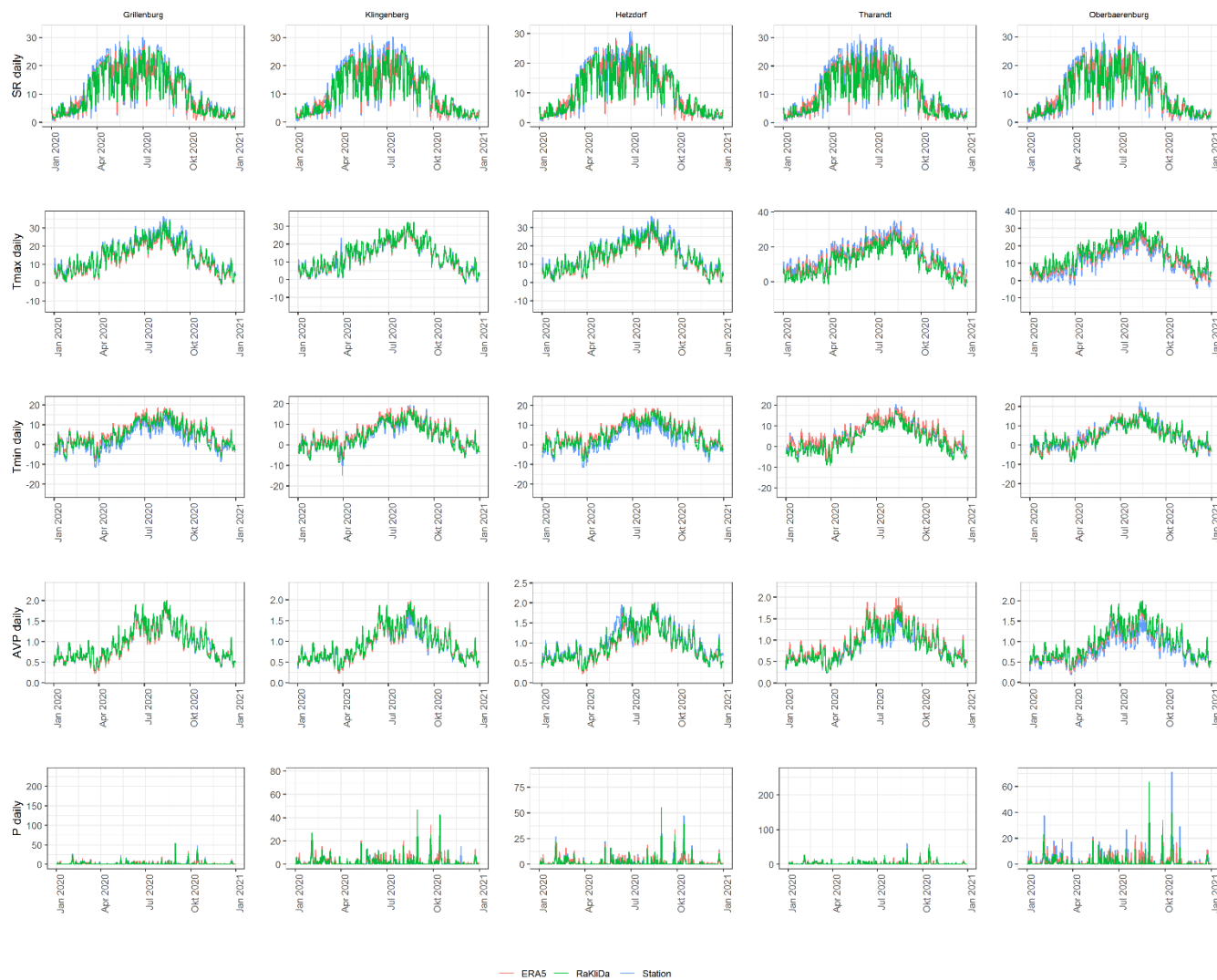


Figure A2 Daily values of meteorological variables for 2020

503
 504
 505



506 **Appendix B. Skill-scores**

Name	Range	Optimum value	Formula
Mean Absolute Error (MAE)	$[0, +\infty]$,	0	$MAE = \frac{\sum_{t=1}^T E_m^t - E_o^t }{T}$ <p>where E_m^t and E_o^t are the modelled and observed evaporation values (in mm) at time t, and T is the overall length of time-series</p>
Nash-Sutcliffe Efficiency (NSE) (Nash and Sutcliffe, 1970b)	$[-\infty, 1]$	1	$NSE = 1 - \frac{\sum_{t=1}^T (E_m^t - E_o^t)^2}{\sum_{t=1}^T (E_o^t - \bar{E}_o)^2}$ <p>where E_m^t and E_o^t are the modelled and observed evaporation values (in mm) at time t, and T is the overall length of time-series</p>
Kling-Gupta Efficiency (KGE) (Gupta et al., 2009b)	$[-\infty, 1]$	1	$KGE = 1 - \sqrt{(r - 1)^2 + (\alpha - 1)^2 + (\beta - 1)^2}$ <p>where r is the Pearson correlation coefficient between the modelled and observed evaporation, α is the ratio between the simulated and observed evaporation variability, β is the ratio between the mean simulated and mean observed evaporation:</p>
	$[-1, 1]$	1	$r = \frac{cov(E_m, E_o)}{\sigma_m \sigma_o} = \frac{\sum_{t=1}^T (E_m^t - \bar{E}_m)(E_o^t - \bar{E}_o)}{\sqrt{\sum_{t=1}^T (E_m^t - \bar{E}_m)^2} \cdot \sqrt{\sum_{t=1}^T (E_o^t - \bar{E}_o)^2}}$
	$[-\infty, +\infty]$	1	$\alpha = \frac{\sqrt{\sum_{t=1}^T (E_m^t - \bar{E}_m)^2}}{\sqrt{\sum_{t=1}^T (E_o^t - \bar{E}_o)^2}}$
	$[-\infty, +\infty]$	1	$\beta = \frac{\bar{E}_m}{\bar{E}_o}$

507

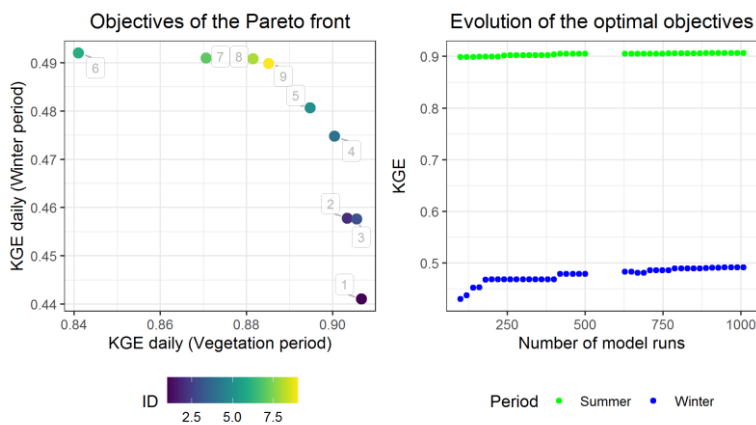


508 **Appendix C. BROOK90 calibration parameters and results**

509 Table C1 Ranges for BROOK90 parameters chosen for the calibration

Parameter abbreviation	Physical meaning	Unit	Range				
			G	K	H	T	O
ALB	albedo or surface reflectivity without snow	-	0.1-0.3	0.1-0.3	0.1-0.3	0.05-0.15	0.07-0.13
ALBSN	albedo or surface reflectivity with snow	-	0.4-0.6	0.4-0.6	0.3-0.5	0.4-0.6	0.35-0.45
CINTRL	maximum interception storage of rain per unit LAI	mm	0.1-0.3	0.1-0.3	0.1-0.3	0.07-0.15	0.10-0.15
CINTSL	maximum interception storage of snow per unit LAI	mm	0.4-0.8	0.4-0.8	0.1-0.6	0.2-0.4	0.1-0.3
CR	extinction coefficient for photosynthetically-active radiation in the canopy	-	0.6-0.8	0.6-0.8	0.5-0.7	0.5-0.7	0.5-0.7
CVPD	vapor pressure deficit at which stomatal conductance is halved	kPa	0.5-2	0.5-2	0.5-2	0.5-2	0.5-2
FRINTL	intercepted fraction of rain per unit LAU	-	0.04-0.1	0.04-0.1	0.01-0.1	0.02-0.06	0.06-0.08
FSINTL	intercepted fraction of snow per unit LAU	-	0.04-0.07	0.01-0.05	0.01-0.1	0.01-0.04	0.02-0.04
GLMAXC	maximum leaf conductance	cm/s	1-1.5	1-1.5	0.3-2	0.3-0.7	0.3-0.6
KSNVP	reduction factor for snow evaporation	-	-	-	0.05-0.5	0.05-0.5	0.05-0.5
LWIDTH	average leaf width	m	0.015-0.025	0.015-0.045	0.02-0.05	0.001-0.003	0.001-0.003
MAXLAI	maximum projected LAI for the year	m ² /m ²	4-6	3-6	5-7	5-8	6-8
MXKPL	maximum plant conductivity	mm day ⁻¹ MPa ⁻¹	7-30	7-30	7-30	7-30	7-30
MXRTLN	maximum length of fine roots per unit ground area	m ² /m ²	600-1000	300-700	1500-4000	1500-2500	2000-3500
PSICR	minimum plant leaf water potential	MPa	-2.5 – -1.5	-2.5 – -1.5	-2.5 – -1.5	-2.5 – -1.5	-2.5 – -1.5
RELHT	pairs of day of the year and relative height between 0 and 1	-	Adjusting relative values for spring and autumn (G,K,H) and for winter (T,O) periods for fixed time-steps				
RELLAI	pairs of day of the year and relative LAI between 0 and 1	-					
IDEPHT	depth over which infiltration is distributed	mm	0-1330	0-800	0-1500	0-1260	0-1020
QFFC	quick flow fraction bypass flow at field capacity	-	0-0.5	0-0.5	0-0.5	0-0.5	0-0.5
QFPAR	fraction of the water content between field capacity and saturation at which the quick flow fraction is 1	-	0-0.5	0-0.5	0-0.5	0-0.5	0-0.5
DRAIN	multiplier between 0 and 1 of drainage from the lowest soil layer	-	0-1	0-1	0-1	0-1	0-1

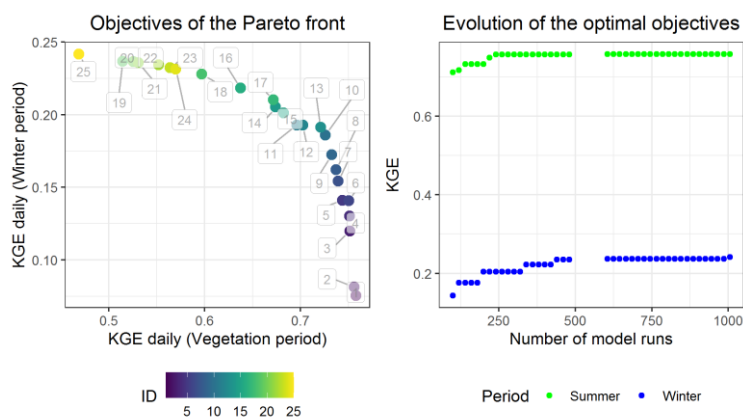
510 Abbreviations for ranges: G – Grillenburg, K – Klingenberg, H – Hetzdorf, T – Tharandt, O – Oberbaerenburg



511

512

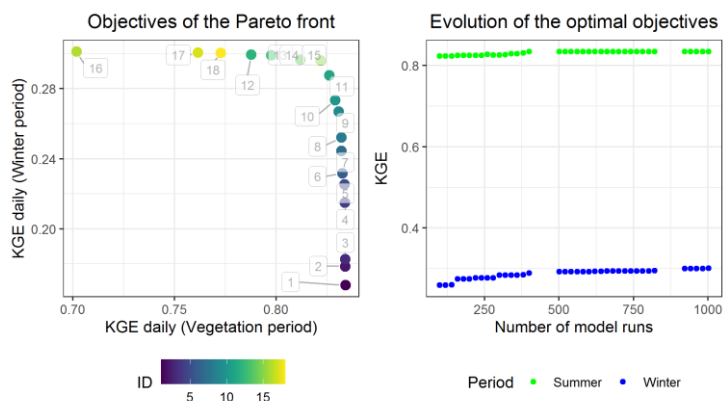
Figure C1 Resulted calibration Pareto fronts for Grillenburg (chosen ID – 9)



513

514

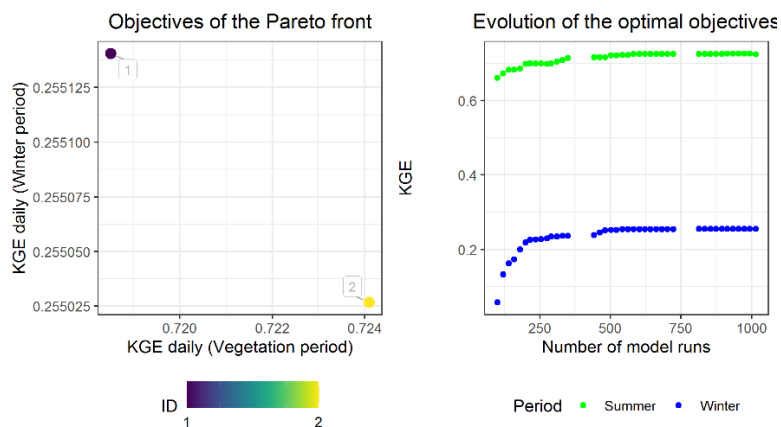
Figure C2 Resulted calibration Pareto fronts for Klingenberg (chosen ID – 13)



515

516

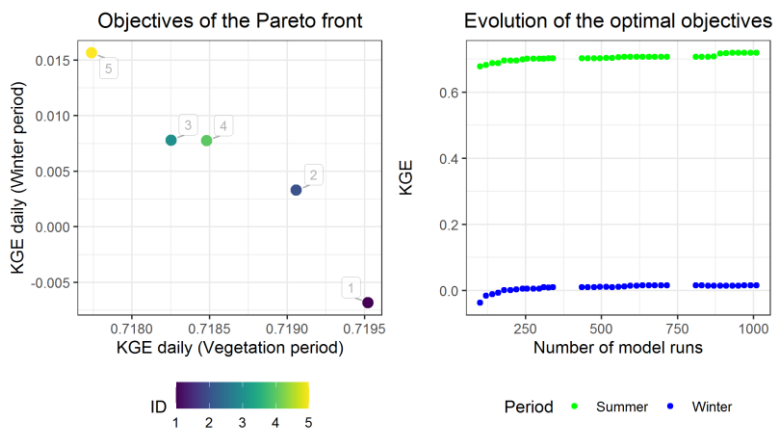
Figure C3 Resulted calibration Pareto fronts for Hetzdorf (chosen ID – 15)



517

518

Figure C4 Resulted calibration Pareto fronts for Tharandt (chosen ID – 2)



519

520

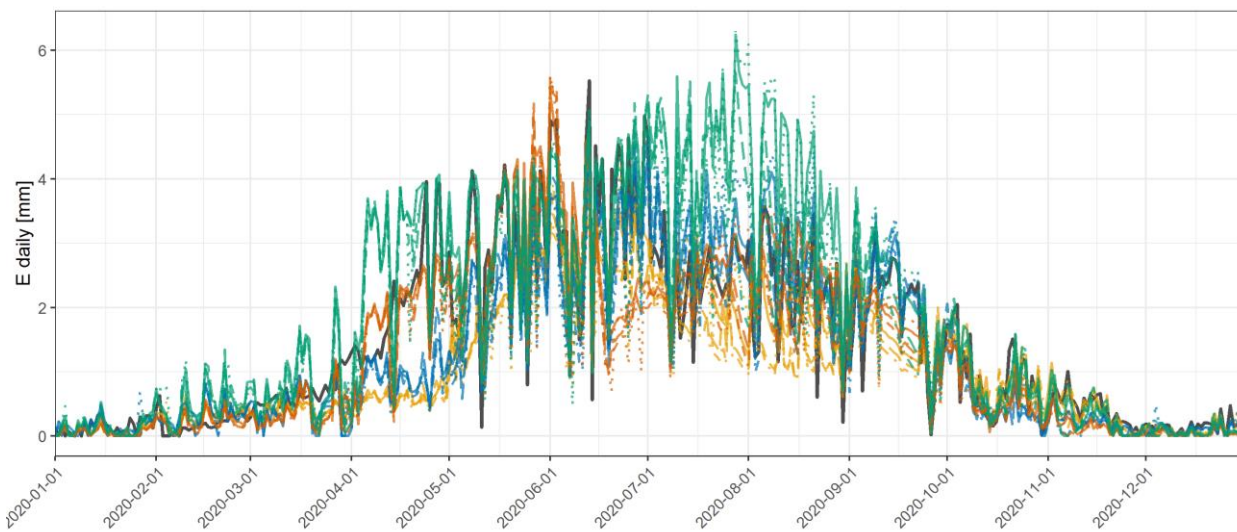
521

Figure C5 Resulted calibration Pareto fronts for Oberbaerenburg (chosen ID – 5)

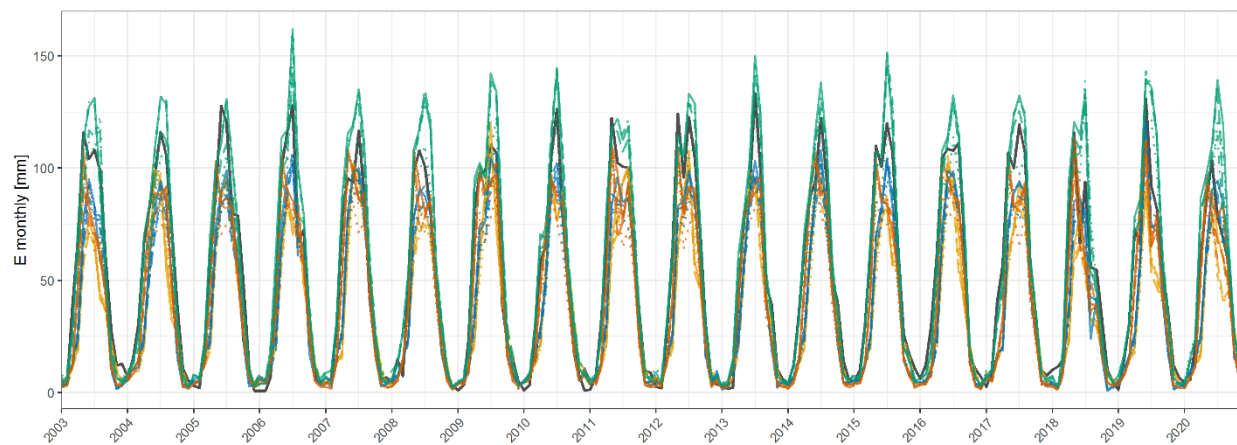


522 **Appendix D. Daily (2020) and monthly (whole time-series) simulations**

523



524



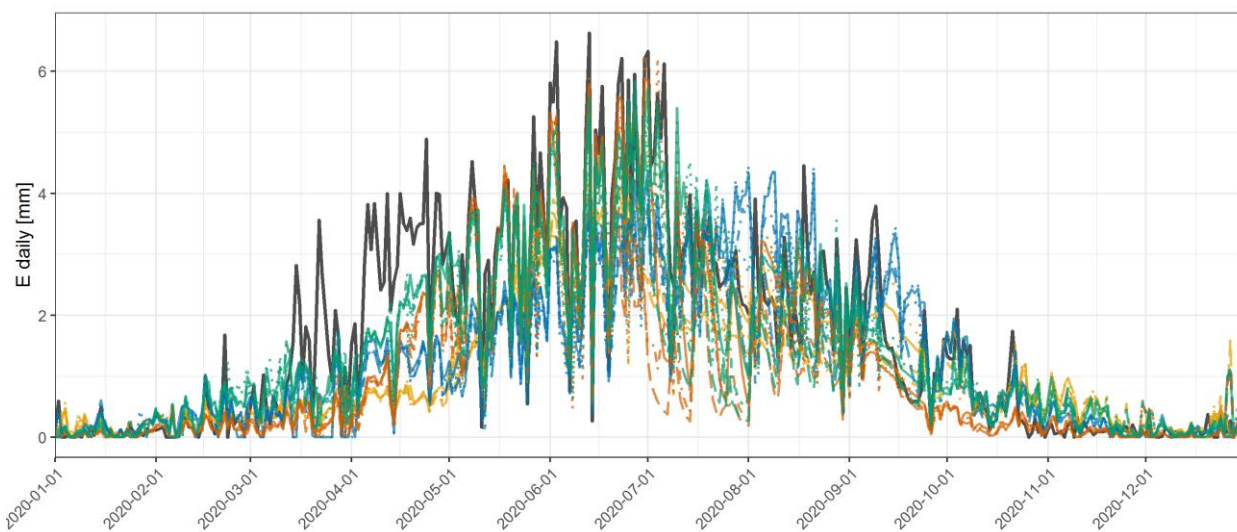
524

525

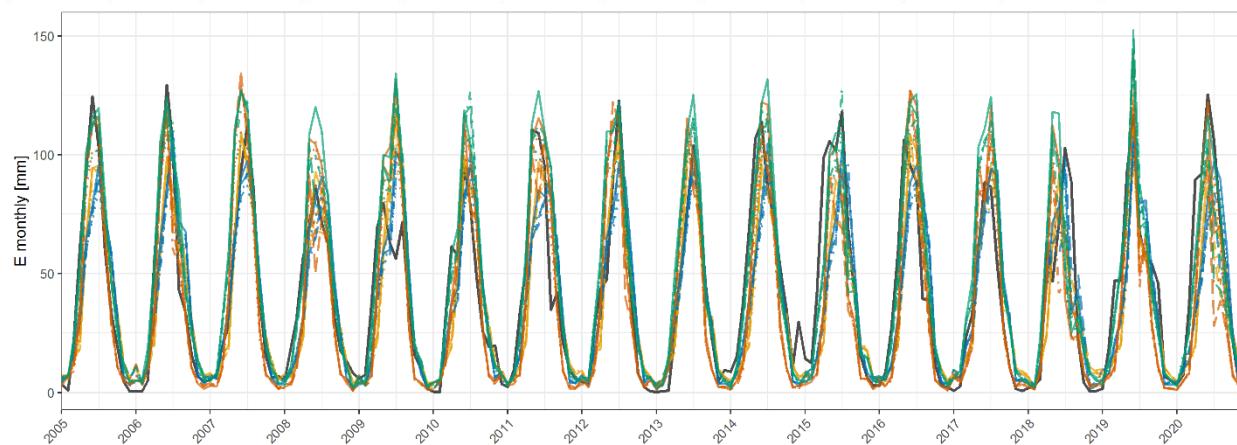
Figure D1 Grillenburg



526



527



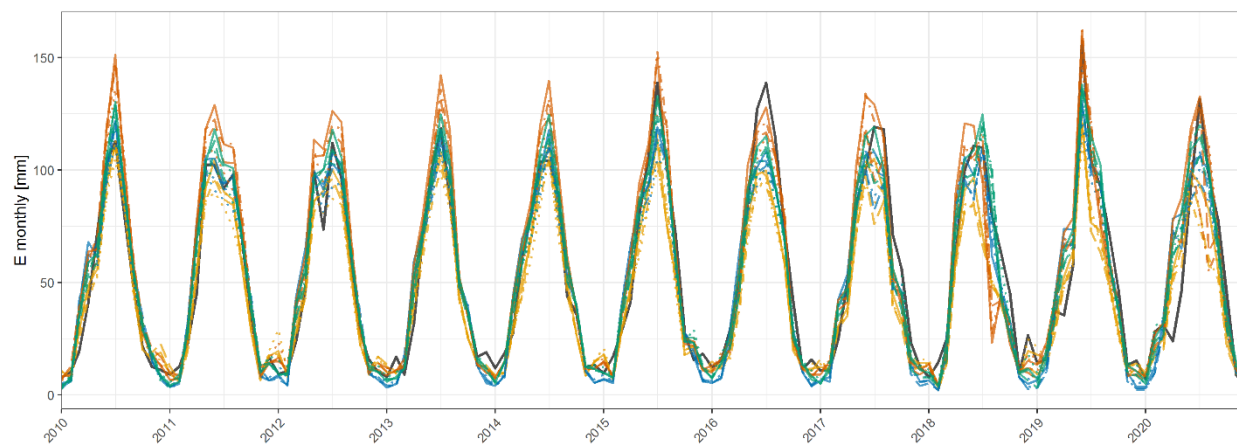
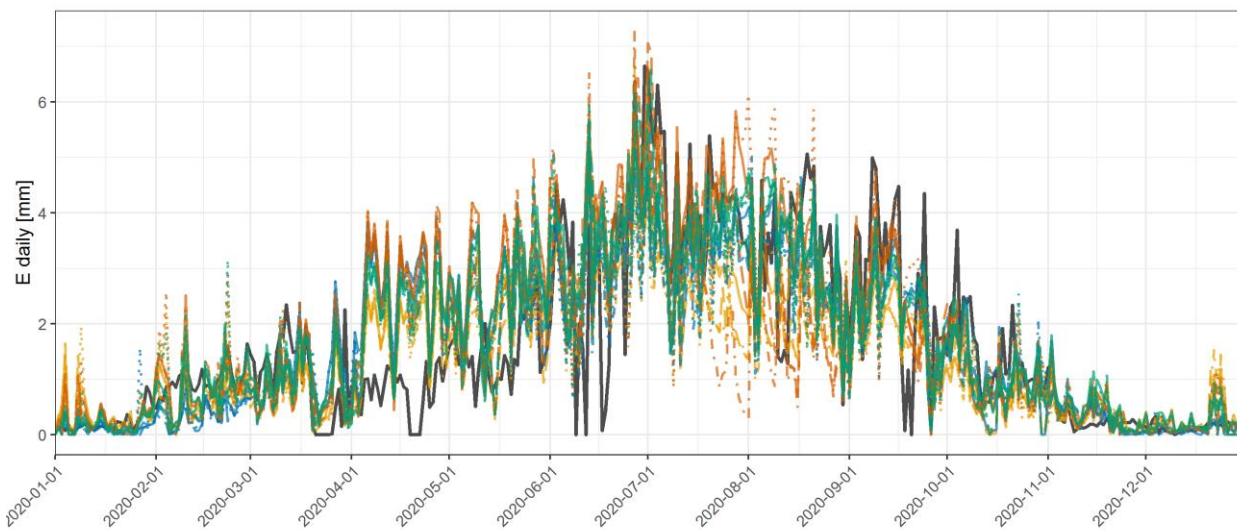
— Measured — GBR90 + station — EXTR + station — BR90 + station — CBR90 + station
 ··· GBR90 + ERA5(hourly) ··· EXTR + ERA5(hourly) ··· BR90 + ERA5(hourly) ··· CBR90 + ERA5(hourly)
 — GBR90 + ERA5(daily) — EXTR + ERA5(daily) — BR90 + ERA5(daily) — CBR90 + ERA5(daily)
 — GBR90 + RAKLIDA — EXTR + RAKLIDA — BR90 + RAKLIDA — CBR90 + RAKLIDA

528

Figure D2 Klingenberg



529



— Measured — GBR90 + station — EXTR + station — BR90 + station — CBR90 + station
 ··· GBR90 + ERA5(hourly) ··· EXTR + ERA5(hourly) ··· BR90 + ERA5(hourly) ··· CBR90 + ERA5(hourly)
 — GBR90 + ERA5(daily) — EXTR + ERA5(daily) — BR90 + ERA5(daily) — CBR90 + ERA5(daily)
 ··· GBR90 + RAKLIDA ··· EXTR + RAKLIDA ··· BR90 + RAKLIDA ··· CBR90 + RAKLIDA

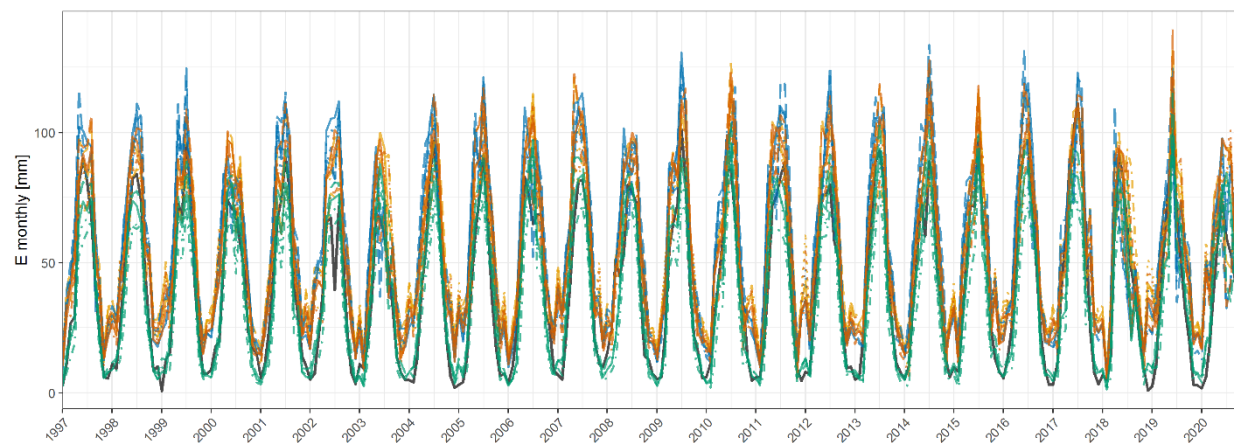
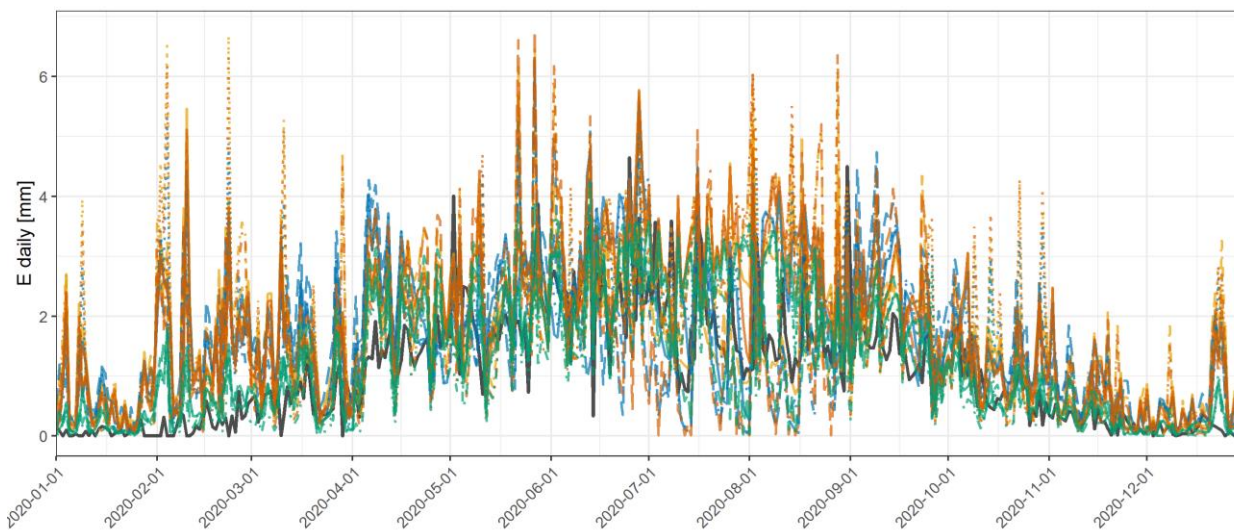
530

531

Figure D3 Hetzdorf



532

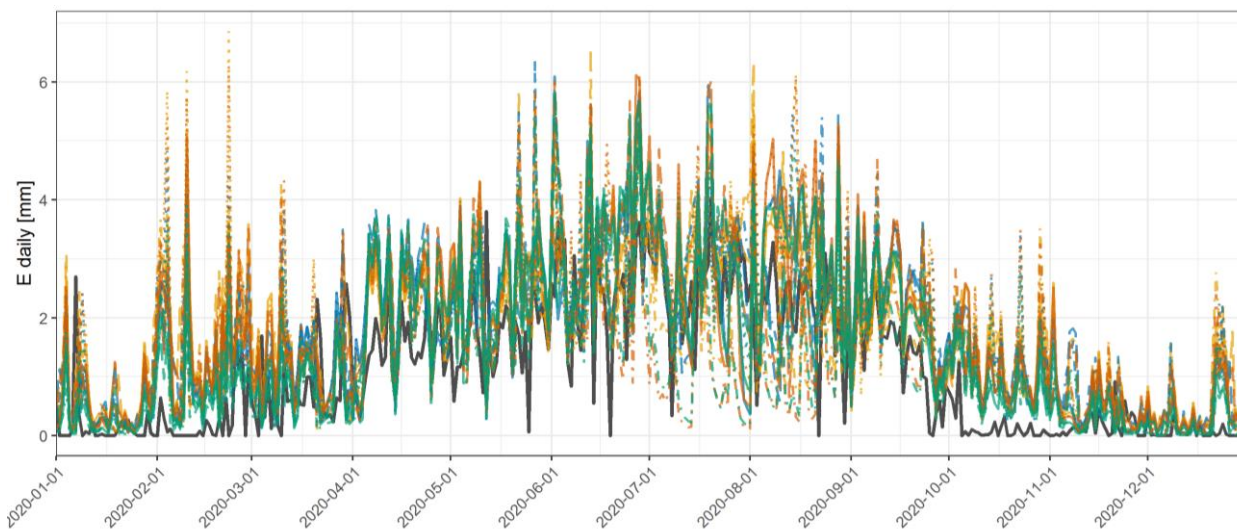


— Measured — GBR90 + station — EXTR + station — BR90 + station — CBR90 + station
 ··· GBR90 + ERA5(hourly) ··· EXTR + ERA5(hourly) ··· BR90 + ERA5(hourly) ··· CBR90 + ERA5(hourly)
 — GBR90 + ERA5(daily) — EXTR + ERA5(daily) — BR90 + ERA5(daily) — CBR90 + ERA5(daily)
 ··· GBR90 + RAKLIDA ··· EXTR + RAKLIDA ··· BR90 + RAKLIDA ··· CBR90 + RAKLIDA

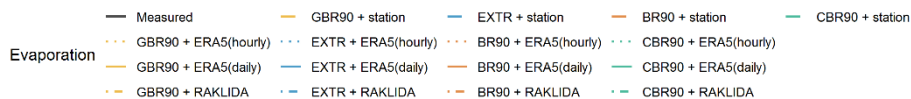
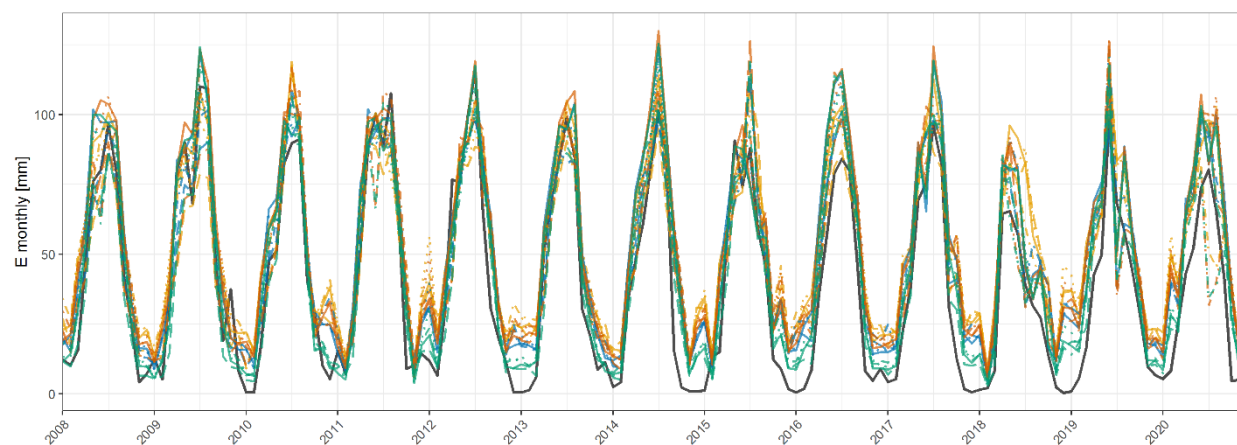
533

534

Figure D4 Tharandt



535



536

537

Figure D5 Oberbaerenburg

538



539 **Appendix E. Evaluation of the simulated evaporation**

540

Table E1. Daily evaporation skill-scores for the whole year

Model/Station	Grillenburg	Klingenberg	Hetzdorf	Tharandt	Oberbaerenburg	
NSE						
GBR90	ERA5 h	0.03	0.2	0.37	0.05	-0.09
	ERA5 d	0.06	0.29	0.56	0.25	0.13
	RaKliDa	-0.05	0.23	0.49	0.09	0.06
	Station	0.08	0.25	0.53	0.23	0.14
EXTR	ERA5 h	0.45	0.32	0.55	0.26	0.19
	ERA5 d	0.57	0.43	0.68	0.38	0.33
	RaKliDa	0.5	0.3	0.65	0.32	0.26
	Station	0.61	0.4	0.69	0.29	0.36
BR90	ERA5 h	0.46	0.53	0.61	0.13	0.09
	ERA5 d	0.61	0.56	0.69	0.36	0.31
	RaKliDa	0.59	0.51	0.67	0.17	0.18
	Station	0.63	0.5	0.71	0.32	0.33
CBR90	ERA5 h	0.76	0.51	0.57	0.48	0.35
	ERA5 d	0.83	0.61	0.72	0.59	0.52
	RaKliDa	0.85	0.59	0.69	0.28	0.41
	Station	0.86	0.6	0.74	0.63	0.53
KGE						
GBR90	ERA5 h	0.36	0.57	0.65	0.45	0.46
	ERA5 d	0.4	0.63	0.74	0.58	0.56
	RaKliDa	0.33	0.58	0.69	0.47	0.52
	Station	0.36	0.6	0.7	0.5	0.57
EXTR	ERA5 h	0.51	0.62	0.77	0.54	0.58
	ERA5 d	0.59	0.7	0.84	0.59	0.63
	RaKliDa	0.53	0.6	0.82	0.57	0.61
	Station	0.59	0.67	0.84	0.52	0.66
BR90	ERA5 h	0.53	0.72	0.78	0.47	0.5
	ERA5 d	0.7	0.76	0.78	0.6	0.6
	RaKliDa	0.65	0.72	0.78	0.51	0.55
	Station	0.66	0.72	0.82	0.52	0.63
CBR90	ERA5 h	0.88	0.76	0.79	0.73	0.66
	ERA5 d	0.84	0.76	0.85	0.79	0.71
	RaKliDa	0.86	0.79	0.85	0.59	0.69
	Station	0.9	0.79	0.86	0.81	0.77
Correlation						
GBR90	ERA5 h	0.78	0.73	0.77	0.54	0.53
	ERA5 d	0.79	0.75	0.83	0.69	0.67
	RaKliDa	0.79	0.75	0.81	0.52	0.59
	Station	0.81	0.75	0.83	0.67	0.62
EXTR	ERA5 h	0.88	0.77	0.79	0.67	0.66
	ERA5 d	0.89	0.78	0.84	0.75	0.73
	RaKliDa	0.89	0.77	0.83	0.68	0.66
	Station	0.9	0.78	0.85	0.69	0.71
BR90	ERA5 h	0.86	0.78	0.79	0.57	0.59



	ERA5 d	0.86	0.77	0.84	0.72	0.71
	RaKliDa	0.87	0.77	0.82	0.55	0.62
	Station	0.89	0.76	0.85	0.68	0.68
CBR90	ERA5 h	0.88	0.77	0.8	0.78	0.71
	ERA5 d	0.92	0.81	0.86	0.82	0.78
	RaKliDa	0.93	0.8	0.85	0.73	0.72
	Station	0.93	0.8	0.87	0.81	0.77
BIAS						
GBR90	ERA5 h	0.69	0.84	0.85	1.38	1.37
	ERA5 d	0.72	0.91	0.89	1.39	1.4
	RaKliDa	0.7	0.87	0.84	1.22	1.35
	Station	0.7	0.87	0.85	1.49	1.23
EXTR	ERA5 h	0.73	0.88	0.94	1.4	1.31
	ERA5 d	0.77	0.94	0.99	1.42	1.35
	RaKliDa	0.73	0.87	0.95	1.34	1.26
	Station	0.75	0.9	0.95	1.44	1.21
BR90	ERA5 h	0.73	0.86	1.03	1.36	1.37
	ERA5 d	0.83	0.94	1.1	1.34	1.38
	RaKliDa	0.8	0.87	1.05	1.17	1.31
	Station	0.8	0.87	1.04	1.41	1.21
CBR90	ERA5 h	0.99	1.06	0.99	0.9	1.19
	ERA5 d	1.13	1.16	1.03	0.94	1.23
	RaKliDa	1.11	1.09	0.98	0.78	1.16
	Station	1.07	1.09	0.98	1.02	1.06
Variance ratio						
GBR90	ERA5 h	0.51	0.62	0.7	1.31	0.95
	ERA5 d	0.5	0.64	0.74	1.15	0.87
	RaKliDa	0.47	0.59	0.76	1.29	0.97
	Station	0.49	0.61	0.74	1.47	0.9
EXTR	ERA5 h	0.59	0.62	0.88	1.32	0.92
	ERA5 d	0.64	0.7	0.98	1.31	0.95
	RaKliDa	0.61	0.61	0.97	1.35	0.97
	Station	0.66	0.66	0.97	1.51	0.94
BR90	ERA5 h	0.63	0.96	1.17	1.42	1.08
	ERA5 d	0.75	1.09	1.31	1.25	1.04
	RaKliDa	0.7	0.97	1.31	1.35	1.08
	Station	0.71	1	1.21	1.61	1.03
CBR90	ERA5 h	0.98	0.91	0.89	0.79	0.94
	ERA5 d	1.18	1.08	1.03	0.86	1.01
	RaKliDa	1.15	0.96	0.99	0.76	0.96
	Station	1.11	1.01	1.02	1.02	0.97
MAE						
GBR90	ERA5 h	0.76	0.69	0.71	0.86	0.97
	ERA5 d	0.72	0.66	0.61	0.77	0.88
	RaKliDa	0.75	0.66	0.67	0.88	0.91
	Station	0.69	0.66	0.62	0.87	0.86
EXTR	ERA5 h	0.64	0.64	0.66	0.81	0.84
	ERA5 d	0.59	0.62	0.59	0.78	0.82
	RaKliDa	0.62	0.64	0.62	0.78	0.81



	Station	0.56	0.62	0.58	0.89	0.76
BR90	ERA5 h	0.64	0.65	0.7	0.85	0.94
	ERA5 d	0.59	0.67	0.65	0.74	0.86
	RaKliDa	0.59	0.66	0.67	0.85	0.92
	Station	0.55	0.67	0.61	0.85	0.82
CBR90	ERA5 h	0.52	0.66	0.64	0.5	0.73
	ERA5 d	0.48	0.64	0.57	0.47	0.69
	RaKliDa	0.46	0.62	0.58	0.6	0.73
	Station	0.42	0.61	0.54	0.5	0.63

Table E2. Daily evaporation skill-scores for the vegetation period

Model/Station	Grillenburg	Klingenberg	Hetzdorf	Tharandt	Oberbaerenburg	
NSE						
GBR90	ERA5 h	-0.46	-0.13	0.09	-0.12	-0.33
	ERA5 d	-0.52	-0.07	0.33	0.06	-0.09
	RaKliDa	-0.64	-0.13	0.28	0	-0.06
	Station	-0.45	-0.08	0.33	0.08	0.04
EXTR	ERA5 h	0.17	-0.08	0.21	0.03	-0.07
	ERA5 d	0.33	0.08	0.4	0.14	0.1
	RaKliDa	0.26	-0.09	0.4	0.15	0.14
	Station	0.41	0.09	0.47	0.12	0.27
BR90	ERA5 h	0.19	0.38	0.43	-0.03	-0.11
	ERA5 d	0.39	0.41	0.53	0.2	0.13
	RaKliDa	0.35	0.37	0.52	0.08	0.08
	Station	0.43	0.37	0.58	0.2	0.26
CBR90	ERA5 h	0.62	0.24	0.3	0.22	0.11
	ERA5 d	0.72	0.37	0.52	0.37	0.32
	RaKliDa	0.75	0.38	0.51	0	0.23
	Station	0.78	0.42	0.59	0.45	0.42
KGE						
GBR90	ERA5 h	0.33	0.49	0.57	0.38	0.39
	ERA5 d	0.34	0.52	0.67	0.54	0.53
	RaKliDa	0.28	0.48	0.64	0.39	0.49
	Station	0.33	0.51	0.66	0.47	0.54
EXTR	ERA5 h	0.51	0.5	0.63	0.48	0.52
	ERA5 d	0.59	0.57	0.71	0.55	0.59
	RaKliDa	0.53	0.49	0.71	0.49	0.58
	Station	0.6	0.56	0.74	0.46	0.64
BR90	ERA5 h	0.53	0.66	0.68	0.39	0.45
	ERA5 d	0.67	0.68	0.71	0.56	0.58
	RaKliDa	0.64	0.66	0.7	0.41	0.51
	Station	0.66	0.65	0.75	0.46	0.61
CBR90	ERA5 h	0.81	0.65	0.67	0.63	0.58
	ERA5 d	0.82	0.68	0.77	0.7	0.67
	RaKliDa	0.84	0.7	0.76	0.51	0.62
	Station	0.87	0.71	0.8	0.71	0.71
Correlation						
GBR90	ERA5 h	0.67	0.61	0.68	0.43	0.43

541



	ERA5 d	0.66	0.63	0.75	0.59	0.6
	RaKliDa	0.67	0.64	0.73	0.42	0.52
	Station	0.71	0.64	0.76	0.58	0.55
EXTR	ERA5 h	0.81	0.66	0.67	0.55	0.56
	ERA5 d	0.83	0.68	0.74	0.64	0.65
	RaKliDa	0.83	0.66	0.73	0.57	0.6
	Station	0.85	0.69	0.76	0.57	0.65
BR90	ERA5 h	0.79	0.7	0.7	0.45	0.49
	ERA5 d	0.78	0.69	0.76	0.62	0.64
	RaKliDa	0.8	0.69	0.74	0.45	0.54
	Station	0.82	0.68	0.78	0.59	0.62
CBR90	ERA5 h	0.81	0.66	0.69	0.67	0.61
	ERA5 d	0.87	0.72	0.78	0.72	0.71
	RaKliDa	0.88	0.72	0.77	0.61	0.64
	Station	0.89	0.72	0.8	0.72	0.71
BIAS						
GBR90	ERA5 h	0.68	0.83	0.83	1.22	1.22
	ERA5 d	0.72	0.9	0.88	1.26	1.27
	RaKliDa	0.68	0.85	0.84	1.07	1.2
	Station	0.69	0.85	0.84	1.34	1.1
EXTR	ERA5 h	0.73	0.88	0.97	1.29	1.22
	ERA5 d	0.77	0.94	1.03	1.32	1.26
	RaKliDa	0.73	0.87	0.99	1.23	1.15
	Station	0.76	0.9	1	1.32	1.11
BR90	ERA5 h	0.74	0.87	1.04	1.23	1.25
	ERA5 d	0.84	0.96	1.12	1.24	1.27
	RaKliDa	0.81	0.88	1.07	1.05	1.18
	Station	0.81	0.88	1.05	1.29	1.1
CBR90	ERA5 h	0.99	1.06	0.99	0.89	1.15
	ERA5 d	1.13	1.17	1.05	0.94	1.2
	RaKliDa	1.11	1.08	1	0.78	1.11
	Station	1.07	1.08	1	1.01	1.03
Variance ratio						
GBR90	ERA5 h	0.55	0.62	0.71	1.32	0.87
	ERA5 d	0.5	0.6	0.72	1.13	0.77
	RaKliDa	0.49	0.57	0.8	1.45	0.97
	Station	0.51	0.6	0.75	1.59	0.91
EXTR	ERA5 h	0.63	0.56	0.75	1.33	0.83
	ERA5 d	0.67	0.61	0.78	1.31	0.85
	RaKliDa	0.65	0.55	0.85	1.48	0.97
	Station	0.7	0.61	0.83	1.68	0.97
BR90	ERA5 h	0.67	1.05	1.2	1.49	1.03
	ERA5 d	0.75	1.15	1.29	1.3	0.99
	RaKliDa	0.72	1.07	1.36	1.59	1.14
	Station	0.72	1.11	1.22	1.84	1.1
CBR90	ERA5 h	0.99	0.83	0.81	0.81	0.86
	ERA5 d	1.1	0.96	0.91	0.85	0.92
	RaKliDa	1.1	0.89	0.93	0.86	0.95
	Station	1.07	0.96	0.96	1.06	1.02



MAE						
GBR90	ERA5 h	1.04	0.91	0.87	0.92	1.05
	ERA5 d	0.98	0.87	0.74	0.83	0.95
	RaKliDa	1.02	0.86	0.83	0.95	0.98
	Station	0.95	0.86	0.76	0.93	0.95
EXTR	ERA5 h	0.86	0.86	0.83	0.91	0.95
	ERA5 d	0.79	0.83	0.73	0.88	0.94
	RaKliDa	0.83	0.85	0.77	0.89	0.9
	Station	0.74	0.82	0.7	1.02	0.85
BR90	ERA5 h	0.85	0.87	0.88	0.93	1.05
	ERA5 d	0.77	0.89	0.82	0.81	0.97
	RaKliDa	0.77	0.88	0.84	0.94	1.03
	Station	0.72	0.89	0.75	0.94	0.91
CBR90	ERA5 h	0.68	0.88	0.8	0.63	0.87
	ERA5 d	0.63	0.85	0.7	0.58	0.83
	RaKliDa	0.59	0.81	0.72	0.76	0.87
	Station	0.53	0.8	0.65	0.61	0.77

542

Table E3. Daily evaporation skill-scores for the winter period

Model/Station	Grillenbug	Klingenberg	Hetzdorf	Tharandt	Oberbaerenburg	
NSE						
GBR90	ERA5 h	-0.86	-2.08	-0.3	-0.42	-0.79
	ERA5 d	-0.7	-1.8	-0.47	-0.56	-1.13
	RaKliDa	-0.56	-1.54	-0.51	-0.36	-0.91
	Station	-0.54	-1.22	-0.5	-0.57	-0.6
EXTR	ERA5 h	-1.05	-2.42	-0.85	-0.44	-0.96
	ERA5 d	-1.13	-2.14	-1.33	-0.52	-1.3
	RaKliDa	-0.98	-1.69	-1.58	-0.42	-0.9
	Station	-1.19	-1.29	-1.6	-0.56	-0.82
BR90	ERA5 h	-2.07	-4.25	-0.29	-0.37	-0.8
	ERA5 d	-1.81	-3.67	-0.37	-0.46	-1.2
	RaKliDa	-1.48	-2.94	-0.41	-0.32	-0.94
	Station	-1.83	-2.13	-0.43	-0.46	-0.67
CBR90	ERA5 h	-0.26	-1.5	-0.16	-0.61	-1.16
	ERA5 d	-0.21	-1.4	-0.41	-0.66	-1.93
	RaKliDa	-0.08	-1.23	-0.4	-0.83	-1.34
	Station	-0.05	-0.96	-0.64	-0.34	-1.6
KGE						
GBR90	ERA5 h	0.24	-0.04	0.15	-0.32	-0.38
	ERA5 d	0.3	0.02	0.25	-0.21	-0.32
	RaKliDa	0.32	0.06	0.17	-0.29	-0.33
	Station	0.34	0.12	0.13	-0.22	-0.2
EXTR	ERA5 h	0.17	-0.13	0.07	-0.22	-0.27
	ERA5 d	0.11	-0.06	-0.1	-0.1	-0.22
	RaKliDa	0.14	0.06	-0.18	-0.14	-0.26
	Station	0.05	0.14	-0.22	-0.14	-0.15
BR90	ERA5 h	-0.22	-0.63	0.22	-0.3	-0.35
	ERA5 d	-0.17	-0.52	0.3	-0.16	-0.28



	RaKliDa	-0.06	-0.32	0.24	-0.26	-0.28
	Station	-0.2	-0.16	0.19	-0.19	-0.17
CBR90	ERA5 h	0.41	0.1	0.32	0.22	-0.16
	ERA5 d	0.43	0.12	0.33	0.26	-0.15
	RaKliDa	0.45	0.15	0.3	0.12	-0.11
	Station	0.49	0.2	0.22	0.26	-0.02
Correlation						
GBR90	ERA5 h	0.33	0.21	0.19	0.14	-0.06
	ERA5 d	0.36	0.24	0.25	0.21	-0.05
	RaKliDa	0.35	0.2	0.19	0.15	-0.02
	Station	0.42	0.22	0.15	0.24	0.13
EXTR	ERA5 h	0.32	0.29	0.28	0.18	-0.04
	ERA5 d	0.27	0.24	0.34	0.27	-0.03
	RaKliDa	0.25	0.25	0.28	0.26	-0.02
	Station	0.32	0.24	0.28	0.29	0.08
BR90	ERA5 h	0.2	0.05	0.24	0.13	-0.07
	ERA5 d	0.19	0.05	0.31	0.21	-0.05
	RaKliDa	0.22	0.03	0.25	0.14	-0.01
	Station	0.29	0.06	0.21	0.23	0.1
CBR90	ERA5 h	0.42	0.26	0.34	0.22	-0.05
	ERA5 d	0.44	0.29	0.37	0.28	-0.03
	RaKliDa	0.46	0.26	0.34	0.15	0.02
	Station	0.5	0.27	0.3	0.28	0.11
BIAS						
GBR90	ERA5 h	0.85	1.15	1.01	3.45	3.92
	ERA5 d	0.9	1.23	0.92	3.15	3.69
	RaKliDa	0.94	1.29	0.88	3.13	3.97
	Station	0.83	1.3	0.9	3.46	3.59
EXTR	ERA5 h	0.76	0.85	0.63	2.91	2.97
	ERA5 d	0.71	0.83	0.55	2.72	2.83
	RaKliDa	0.74	0.95	0.53	2.79	3.11
	Station	0.65	0.98	0.51	3.1	2.91
BR90	ERA5 h	0.57	0.56	0.97	3.15	3.49
	ERA5 d	0.59	0.57	0.9	2.75	3.16
	RaKliDa	0.62	0.64	0.88	2.76	3.46
	Station	0.56	0.69	0.9	3.01	3.11
CBR90	ERA5 h	1.05	1.12	0.96	1.01	2
	ERA5 d	1	1.11	0.81	0.98	1.78
	RaKliDa	1.1	1.2	0.8	0.82	2.01
	Station	0.96	1.24	0.75	1.21	1.62
Variance ratio						
GBR90	ERA5 h	0.59	0.36	1.7	11.57	3.47
	ERA5 d	0.63	0.4	1.05	6.56	2.15
	RaKliDa	0.73	0.49	1.19	10.35	2.86
	Station	0.65	0.57	1.35	7.88	2.87
EXTR	ERA5 h	0.54	0.29	0.85	6.8	1.88
	ERA5 d	0.57	0.34	0.61	4.38	1.26
	RaKliDa	0.65	0.41	0.6	5.53	2.02
	Station	0.52	0.51	0.61	5.61	1.74



BR90	ERA5 h	0.42	0.24	1.43	10.51	2.91
	ERA5 d	0.47	0.27	1.03	5.42	1.64
	RaKliDa	0.53	0.34	1.17	8.52	2.23
	Station	0.42	0.45	1.27	6.6	2.21
CBR90	ERA5 h	0.86	0.44	1.37	0.93	1.1
	ERA5 d	0.86	0.44	0.88	0.78	0.6
	RaKliDa	1.02	0.52	0.98	0.89	0.86
	Station	0.92	0.62	0.86	1.22	0.56
MAE						
GBR90	ERA5 h	0.19	0.23	0.36	0.75	0.8
	ERA5 d	0.19	0.23	0.32	0.67	0.74
	RaKliDa	0.19	0.24	0.34	0.73	0.78
	Station	0.18	0.24	0.36	0.74	0.69
EXTR	ERA5 h	0.19	0.19	0.31	0.61	0.61
	ERA5 d	0.2	0.2	0.31	0.55	0.58
	RaKliDa	0.2	0.2	0.32	0.57	0.64
	Station	0.19	0.21	0.32	0.65	0.57
BR90	ERA5 h	0.21	0.21	0.33	0.69	0.72
	ERA5 d	0.21	0.22	0.3	0.58	0.65
	RaKliDa	0.21	0.22	0.33	0.66	0.69
	Station	0.2	0.23	0.34	0.64	0.62
CBR90	ERA5 h	0.2	0.22	0.31	0.25	0.45
	ERA5 d	0.19	0.21	0.28	0.24	0.41
	RaKliDa	0.19	0.22	0.29	0.26	0.44
	Station	0.18	0.23	0.3	0.27	0.36

543

Table E4. Monthly evaporation skill-scores for the whole year

Model/Station	Grillenbug	Klingenberg	Hetzdorf	Tharandt	Oberbaerenburg	
NSE						
GBR90	ERA5 h	0.37	0.56	0.74	0.44	0.49
	ERA5 d	0.49	0.65	0.84	0.57	0.59
	RaKliDa	0.37	0.59	0.78	0.54	0.54
	Station	0.4	0.56	0.77	0.47	0.55
EXTR	ERA5 h	0.63	0.61	0.84	0.59	0.7
	ERA5 d	0.74	0.68	0.88	0.61	0.71
	RaKliDa	0.66	0.55	0.88	0.63	0.72
	Station	0.72	0.6	0.89	0.48	0.75
BR90	ERA5 h	0.65	0.77	0.89	0.57	0.63
	ERA5 d	0.84	0.77	0.88	0.69	0.69
	RaKliDa	0.8	0.74	0.88	0.67	0.63
	Station	0.81	0.72	0.9	0.6	0.72
CBR90	ERA5 h	0.93	0.83	0.9	0.84	0.84
	ERA5 d	0.92	0.79	0.92	0.9	0.85
	RaKliDa	0.93	0.81	0.92	0.67	0.83
	Station	0.93	0.79	0.93	0.91	0.87
KGE						
GBR90	ERA5 h	0.41	0.68	0.66	0.67	0.65
	ERA5 d	0.51	0.79	0.79	0.71	0.69



	RaKliDa	0.43	0.72	0.71	0.69	0.66
	Station	0.44	0.72	0.72	0.67	0.67
EXTR	ERA5 h	0.54	0.71	0.86	0.71	0.74
	ERA5 d	0.65	0.82	0.94	0.69	0.74
	RaKliDa	0.57	0.7	0.91	0.73	0.75
	Station	0.62	0.75	0.92	0.67	0.77
BR90	ERA5 h	0.54	0.8	0.94	0.72	0.71
	ERA5 d	0.76	0.82	0.84	0.74	0.72
	RaKliDa	0.7	0.8	0.89	0.76	0.72
	Station	0.7	0.8	0.91	0.7	0.77
CBR90	ERA5 h	0.96	0.9	0.89	0.82	0.83
	ERA5 d	0.82	0.79	0.94	0.91	0.8
	RaKliDa	0.85	0.86	0.95	0.65	0.84
	Station	0.88	0.85	0.96	0.95	0.91
Correlation						
GBR90	ERA5 h	0.92	0.86	0.96	0.91	0.91
	ERA5 d	0.91	0.86	0.95	0.94	0.94
	RaKliDa	0.91	0.85	0.96	0.89	0.93
	Station	0.91	0.84	0.95	0.94	0.89
EXTR	ERA5 h	0.95	0.87	0.94	0.93	0.94
	ERA5 d	0.95	0.86	0.94	0.93	0.94
	RaKliDa	0.95	0.85	0.95	0.92	0.94
	Station	0.95	0.85	0.95	0.89	0.93
BR90	ERA5 h	0.96	0.9	0.95	0.92	0.93
	ERA5 d	0.96	0.88	0.95	0.94	0.94
	RaKliDa	0.96	0.88	0.94	0.9	0.91
	Station	0.96	0.87	0.95	0.93	0.92
CBR90	ERA5 h	0.97	0.92	0.96	0.95	0.95
	ERA5 d	0.98	0.91	0.96	0.95	0.95
	RaKliDa	0.98	0.91	0.96	0.93	0.94
	Station	0.97	0.9	0.96	0.96	0.94
BIAS						
GBR90	ERA5 h	0.69	0.84	0.85	1.38	1.37
	ERA5 d	0.72	0.91	0.89	1.39	1.4
	RaKliDa	0.7	0.87	0.84	1.22	1.35
	Station	0.7	0.87	0.85	1.49	1.23
EXTR	ERA5 h	0.73	0.88	0.94	1.4	1.31
	ERA5 d	0.77	0.94	0.99	1.42	1.35
	RaKliDa	0.73	0.87	0.95	1.34	1.26
	Station	0.75	0.9	0.95	1.44	1.21
BR90	ERA5 h	0.73	0.86	1.03	1.36	1.37
	ERA5 d	0.83	0.94	1.1	1.34	1.38
	RaKliDa	0.8	0.87	1.05	1.17	1.31
	Station	0.8	0.87	1.04	1.41	1.21
CBR90	ERA5 h	0.99	1.06	0.99	0.9	1.19
	ERA5 d	1.13	1.16	1.03	0.94	1.23
	RaKliDa	1.11	1.09	0.98	0.78	1.16
	Station	1.07	1.09	0.98	1.02	1.06
Variance ratio						



GBR90	ERA5 h	0.53	0.67	0.61	0.75	0.69
	ERA5 d	0.6	0.8	0.74	0.91	0.81
	RaKliDa	0.54	0.71	0.68	0.66	0.68
	Station	0.56	0.73	0.68	1	0.64
EXTR	ERA5 h	0.62	0.68	0.81	1.01	0.84
	ERA5 d	0.73	0.82	1	1.16	0.97
	RaKliDa	0.66	0.68	0.92	0.98	0.78
	Station	0.71	0.72	0.94	1.09	0.76
BR90	ERA5 h	0.61	1.03	1.03	0.88	0.87
	ERA5 d	0.82	1.28	1.3	1.03	0.99
	RaKliDa	0.75	1.1	1.19	0.75	0.8
	Station	0.76	1.1	1.13	1.1	0.8
CBR90	ERA5 h	0.97	1.01	0.83	0.79	0.95
	ERA5 d	1.36	1.32	1.06	0.9	1.12
	RaKliDa	1.28	1.12	0.95	0.7	0.91
	Station	1.23	1.15	1.01	0.98	0.93
MAE						
GBR90	ERA5 h	17.04	13.93	11.7	16.25	16.99
	ERA5 d	15.94	13.78	9.95	16.05	16.91
	RaKliDa	17.17	14.09	11.05	13.05	16.15
	Station	16.9	14.71	11.22	19.56	15.01
EXTR	ERA5 h	15.12	13.21	10.08	16.85	14.43
	ERA5 d	13.59	13.37	9.82	17.6	15.15
	RaKliDa	14.75	14.32	9.69	15.5	13.14
	Station	13.77	13.93	9.32	19.99	12.26
BR90	ERA5 h	14.6	12.81	9.48	15.45	16.49
	ERA5 d	11.31	13.91	11.25	14.38	15.96
	RaKliDa	12.11	14.09	10.67	11.8	15.29
	Station	11.86	14.47	9.8	17.32	13.02
CBR90	ERA5 h	7.08	10.51	8.36	7.7	10.74
	ERA5 d	9.12	12.59	8.39	6.69	11.16
	RaKliDa	8.24	11.56	8.01	10.93	10.51
	Station	7.9	12.11	7.9	6.35	8.85

544

Table E5. Monthly evaporation skill-scores for the vegetation period

Model/Station	Grillenbug	Klingenberg	Hetzdorf	Tharandt	Oberbaerenburg	
NSE						
GBR90	ERA5 h	-0.18	0.23	0.5	0.32	0.3
	ERA5 d	0.07	0.4	0.69	0.4	0.41
	RaKliDa	-0.14	0.3	0.58	0.57	0.43
	Station	-0.1	0.27	0.56	0.22	0.48
EXTR	ERA5 h	0.3	0.17	0.59	0.3	0.5
	ERA5 d	0.54	0.35	0.71	0.29	0.49
	RaKliDa	0.39	0.11	0.72	0.42	0.65
	Station	0.49	0.21	0.74	0.13	0.68
BR90	ERA5 h	0.29	0.64	0.78	0.45	0.48
	ERA5 d	0.69	0.65	0.75	0.55	0.53
	RaKliDa	0.62	0.62	0.77	0.68	0.51



	Station	0.63	0.59	0.81	0.41	0.68
CBR90	ERA5 h	0.86	0.66	0.75	0.68	0.72
	ERA5 d	0.83	0.61	0.83	0.79	0.71
	RaKliDa	0.86	0.65	0.84	0.39	0.7
	Station	0.86	0.62	0.86	0.83	0.8
KGE						
GBR90	ERA5 h	0.45	0.63	0.62	0.72	0.62
	ERA5 d	0.54	0.71	0.76	0.77	0.7
	RaKliDa	0.47	0.66	0.69	0.78	0.66
	Station	0.48	0.65	0.7	0.73	0.69
EXTR	ERA5 h	0.59	0.58	0.63	0.74	0.72
	ERA5 d	0.68	0.69	0.78	0.72	0.75
	RaKliDa	0.61	0.58	0.74	0.76	0.76
	Station	0.66	0.62	0.77	0.67	0.79
BR90	ERA5 h	0.57	0.76	0.89	0.78	0.74
	ERA5 d	0.78	0.72	0.82	0.78	0.76
	RaKliDa	0.73	0.72	0.85	0.84	0.75
	Station	0.74	0.71	0.89	0.73	0.82
CBR90	ERA5 h	0.93	0.83	0.75	0.81	0.82
	ERA5 d	0.79	0.75	0.9	0.89	0.82
	RaKliDa	0.82	0.8	0.87	0.67	0.83
	Station	0.85	0.78	0.91	0.91	0.9
Correlation						
GBR90	ERA5 h	0.85	0.75	0.92	0.87	0.88
	ERA5 d	0.83	0.74	0.92	0.91	0.91
	RaKliDa	0.83	0.74	0.92	0.84	0.89
	Station	0.83	0.72	0.91	0.9	0.84
EXTR	ERA5 h	0.91	0.75	0.9	0.87	0.91
	ERA5 d	0.91	0.74	0.9	0.87	0.91
	RaKliDa	0.91	0.7	0.91	0.85	0.91
	Station	0.91	0.71	0.91	0.79	0.89
BR90	ERA5 h	0.93	0.83	0.9	0.88	0.9
	ERA5 d	0.92	0.81	0.9	0.91	0.91
	RaKliDa	0.92	0.81	0.89	0.85	0.86
	Station	0.93	0.79	0.91	0.88	0.88
CBR90	ERA5 h	0.93	0.84	0.92	0.89	0.92
	ERA5 d	0.95	0.83	0.93	0.91	0.92
	RaKliDa	0.95	0.83	0.93	0.87	0.89
	Station	0.94	0.81	0.93	0.91	0.91
BIAS						
GBR90	ERA5 h	0.68	0.83	0.83	1.22	1.22
	ERA5 d	0.72	0.9	0.88	1.26	1.27
	RaKliDa	0.68	0.85	0.84	1.07	1.2
	Station	0.69	0.85	0.84	1.34	1.1
EXTR	ERA5 h	0.73	0.88	0.97	1.29	1.22
	ERA5 d	0.77	0.94	1.03	1.32	1.26
	RaKliDa	0.73	0.87	0.99	1.23	1.15
	Station	0.76	0.9	1	1.32	1.11
BR90	ERA5 h	0.74	0.87	1.04	1.23	1.25



	ERA5 d	0.84	0.96	1.12	1.24	1.27
	RaKliDa	0.81	0.88	1.07	1.05	1.18
	Station	0.81	0.88	1.06	1.29	1.1
CBR90	ERA5 h	0.99	1.06	0.99	0.89	1.15
	ERA5 d	1.13	1.17	1.05	0.94	1.2
	RaKliDa	1.11	1.08	1	0.78	1.11
	Station	1.07	1.08	1	1.01	1.03
Variance ratio						
GBR90	ERA5 h	0.64	0.71	0.58	0.73	0.58
	ERA5 d	0.74	0.86	0.72	0.91	0.7
	RaKliDa	0.69	0.79	0.67	0.77	0.61
	Station	0.69	0.82	0.67	1.03	0.64
EXTR	ERA5 h	0.73	0.59	0.55	0.97	0.7
	ERA5 d	0.9	0.75	0.7	1.14	0.82
	RaKliDa	0.82	0.64	0.65	1.01	0.73
	Station	0.87	0.68	0.68	1.15	0.75
BR90	ERA5 h	0.67	1.23	0.95	0.91	0.78
	ERA5 d	0.91	1.55	1.23	1.1	0.91
	RaKliDa	0.85	1.37	1.15	0.92	0.78
	Station	0.84	1.37	1.07	1.22	0.86
CBR90	ERA5 h	0.97	0.93	0.66	0.83	0.84
	ERA5 d	1.42	1.29	0.9	0.95	1.01
	RaKliDa	1.35	1.11	0.81	0.84	0.84
	Station	1.31	1.17	0.89	1.03	0.96
MAE						
GBR90	ERA5 h	24.02	18.64	15.24	14.33	15.87
	ERA5 d	22.44	18.33	12.84	15.23	16.54
	RaKliDa	24.23	18.65	14.4	10.68	14.7
	Station	23.78	19.65	14.38	19.24	13.97
EXTR	ERA5 h	20.8	18.05	12.28	17.44	14.9
	ERA5 d	18.27	18.12	11.52	19.34	16.42
	RaKliDa	20.12	19.52	11.16	15.93	12.55
	Station	18.67	18.98	10.45	21.39	11.88
BR90	ERA5 h	19.72	17.03	12.24	14.3	16.36
	ERA5 d	14.77	18.62	15	14.32	16.64
	RaKliDa	15.99	18.86	13.95	10.23	14.91
	Station	15.58	19.57	12.45	17.71	12.43
CBR90	ERA5 h	9.07	13.66	10.68	9.82	11.91
	ERA5 d	12.11	16.86	10.55	8.35	13.09
	RaKliDa	10.8	15.2	9.89	14.54	11.77
	Station	10.35	16.02	9.58	7.76	10.19

Table E6. Monthly evaporation skill-scores for the winter period

Model/Station	Grillenbug	Klingenberg	Hetzdorf	Tharandt	Oberbaerenburg	
NSE						
GBR90	ERA5 h	-0.84	-3.36	-0.21	-3.65	-3.23
	ERA5 d	-0.62	-2.97	-0.56	-4.55	-4.59
	RaKliDa	-0.48	-2.77	-0.88	-3.28	-4.82



	Station	-0.46	-2.6	-1.21	-6.21	-4.03
EXTR	ERA5 h	-4.44	-5.59	-2.96	-3.47	-3.15
	ERA5 d	-4.71	-6.57	-4.39	-3.68	-3.9
	RaKliDa	-3.93	-5.71	-4.81	-3.62	-3.5
	Station	-4.19	-4.8	-4.49	-5.1	-3.8
BR90	ERA5 h	-8.08	-16.29	-0.02	-3.13	-3
	ERA5 d	-7.88	-14.62	-0.18	-3.66	-4.2
	RaKliDa	-6.26	-9.67	-0.45	-2.75	-4.27
	Station	-6.69	-7.49	-0.91	-4.85	-3.74
CBR90	ERA5 h	-0.4	-1.97	0.27	-0.86	-1.95
	ERA5 d	-0.49	-2.02	-0.21	-0.83	-2.61
	RaKliDa	-0.35	-2.27	-0.23	-2.12	-2.36
	Station	-0.22	-2.08	-0.96	-0.45	-2.65
KGE						
GBR90	ERA5 h	0.27	-0.3	0.32	-0.32	-0.32
	ERA5 d	0.33	-0.21	0.35	-0.22	-0.28
	RaKliDa	0.39	-0.15	0.27	-0.34	-0.2
	Station	0.4	-0.11	0.09	-0.16	-0.27
EXTR	ERA5 h	-0.45	-0.86	0.02	-0.17	-0.16
	ERA5 d	-0.44	-0.97	-0.17	-0.08	-0.14
	RaKliDa	-0.33	-0.8	-0.26	-0.02	-0.23
	Station	-0.35	-0.66	-0.3	-0.02	-0.18
BR90	ERA5 h	-0.84	-1.98	0.47	-0.29	-0.27
	ERA5 d	-0.82	-1.8	0.48	-0.16	-0.23
	RaKliDa	-0.63	-1.2	0.4	-0.3	-0.15
	Station	-0.68	-0.95	0.22	-0.09	-0.23
CBR90	ERA5 h	0.42	-0.01	0.58	0.27	-0.05
	ERA5 d	0.38	-0.04	0.49	0.28	-0.07
	RaKliDa	0.44	-0.07	0.47	0	0.05
	Station	0.47	-0.02	0.29	0.42	-0.08
Correlation						
GBR90	ERA5 h	0.54	0.2	0.33	0.05	0
	ERA5 d	0.56	0.23	0.37	0.1	-0.01
	RaKliDa	0.51	0.15	0.31	-0.01	0.11
	Station	0.55	0.21	0.11	0.21	0
EXTR	ERA5 h	0.27	0.39	0.3	0.16	0.07
	ERA5 d	0.06	0.29	0.29	0.22	0.06
	RaKliDa	0.16	0.23	0.2	0.33	-0.01
	Station	0.29	0.29	0.17	0.35	0.03
BR90	ERA5 h	0.21	0.06	0.47	0.07	0.01
	ERA5 d	0.17	0.03	0.5	0.13	-0.01
	RaKliDa	0.15	-0.11	0.42	-0.01	0.12
	Station	0.25	0.01	0.25	0.24	-0.01
CBR90	ERA5 h	0.52	0.32	0.6	0.35	0.07
	ERA5 d	0.52	0.36	0.55	0.37	0.07
	RaKliDa	0.55	0.29	0.53	0.24	0.21
	Station	0.56	0.33	0.39	0.46	0.09
BIAS						
GBR90	ERA5 h	0.85	1.15	1.01	3.45	3.93



	ERA5 d	0.9	1.23	0.92	3.16	3.69
	RaKliDa	0.94	1.29	0.88	3.14	3.97
	Station	0.83	1.3	0.9	3.46	3.59
EXTR	ERA5 h	0.76	0.85	0.63	2.91	2.97
	ERA5 d	0.71	0.83	0.54	2.72	2.83
	RaKliDa	0.74	0.95	0.53	2.79	3.11
	Station	0.65	0.98	0.51	3.1	2.91
BR90	ERA5 h	0.57	0.55	0.97	3.15	3.49
	ERA5 d	0.59	0.57	0.9	2.76	3.16
	RaKliDa	0.63	0.64	0.88	2.76	3.47
	Station	0.55	0.69	0.9	3.01	3.11
CBR90	ERA5 h	1.05	1.12	0.96	1.01	2
	ERA5 d	1	1.11	0.81	0.98	1.78
	RaKliDa	1.1	1.2	0.8	0.82	2.01
	Station	0.96	1.24	0.75	1.21	1.62
Variance ratio						
GBR90	ERA5 h	0.42	0.24	1.27	5.85	3.09
	ERA5 d	0.45	0.28	0.73	3.64	1.88
	RaKliDa	0.54	0.33	0.68	5.09	2.07
	Station	0.56	0.33	0.74	3.39	2
EXTR	ERA5 h	0.2	0.13	0.55	3.71	1.55
	ERA5 d	0.24	0.13	0.5	2.83	1.12
	RaKliDa	0.26	0.15	0.51	2.99	1.63
	Station	0.25	0.16	0.58	2.92	1.25
BR90	ERA5 h	0.16	0.07	1.08	5.28	2.5
	ERA5 d	0.17	0.08	0.84	3.05	1.42
	RaKliDa	0.2	0.13	0.8	4.22	1.66
	Station	0.19	0.15	0.72	2.91	1.53
CBR90	ERA5 h	0.57	0.33	1.3	0.56	0.97
	ERA5 d	0.52	0.3	0.96	0.55	0.59
	RaKliDa	0.57	0.32	1.01	0.38	0.73
	Station	0.61	0.33	0.83	0.76	0.48
MAE						
GBR90	ERA5 h	3.08	4.51	4.6	20.09	19.24
	ERA5 d	2.95	4.69	4.17	17.68	17.65
	RaKliDa	3.04	4.97	4.34	17.78	19.04
	Station	3.13	4.83	4.92	20.19	17.09
EXTR	ERA5 h	3.77	3.54	5.67	15.67	13.5
	ERA5 d	4.23	3.86	6.42	14.12	12.6
	RaKliDa	4.03	3.92	6.77	14.66	14.33
	Station	3.96	3.82	7.07	17.21	13.04
BR90	ERA5 h	4.36	4.36	3.96	17.76	16.74
	ERA5 d	4.39	4.48	3.76	14.49	14.61
	RaKliDa	4.33	4.55	4.11	14.92	16.07
	Station	4.42	4.27	4.49	16.53	14.22
CBR90	ERA5 h	3.1	4.21	3.72	3.46	8.4
	ERA5 d	3.14	4.05	4.07	3.38	7.31
	RaKliDa	3.13	4.28	4.23	3.71	8
	Station	2.99	4.27	4.54	3.53	6.18



546 **Data and Code availability**

547 Authors fully support open-source and reproducible research. Therefore, all the data and codes are available as
548 Supplementary material under the following HydroShare composite resource
549 <https://doi.org/10.4211/hs.567d7bdc7b84465ca333b6e0c011853a>, which include:

- 550 - Raw eddy-covariance and meteorological measurement daily data with location files
- 551 - Raw results of model runs for each framework, including model calibration and FAO simulations
- 552 - R-scripts to reproduce figures and tables for the manuscript

553 In addition, Global BROOK90 framework is available under https://github.com/hydrovorobey/Global_BROOK90,
554 EXTRUSO framework is available under https://github.com/GeoinformationSystems/xtruso_R, and BROOK90 R-version is
555 available under https://github.com/rkronen/Brook90_R.

556 **Author contribution**

557 Conceptualization VI, LTT and KR; data curation GT, LTT and VI, formal analysis VI, funding acquisition BC,
558 methodology VI, LTT and KR; supervision KR; visualization VI; writing: original draft preparation VI and LTT, writing:
559 review KR, GT, BC.

560 **Competing interests**

561 The authors declare that they have no conflict of interest.

562 **Acknowledgements**

563 Authors would like to express great thanks to Uwe Spank for his valuable advises and comments to the paper draft.
564 Additionally, authors thank BMBF for providing the funding opportunities for the study under the scope of the
565 'KlimaKonform' project.

566 **References**

- 567 1. Ad-hoc-AG Boden: Bodenkundliche Kartieranleitung, Bundesanstalt für Geowissenschaften und Rohstoffe in
568 Zusammenarbeit mit den Staatlichen Geologischen Dienstender Bundesrepublik Deutschland, Hannover, 2005.
- 569 2. Allen, R., Pereira, L., Raes, D., and Smith, M.: Crop evapotranspiration - Guidelines for computing crop water
570 requirements - FAO Irrigation and drainage paper 56, FAO - Food and Agriculture Organization of the United Nations,
571 Rome, 1998.



- 572 3. Anderson, M. C., Norman, J. M., Mecikalski, J. R., Otkin, J. A., and Kustas, W. P.: A climatological study of
573 evapotranspiration and moisture stress across the continental United States based on thermal remote sensing: 1. Model
574 formulation, 112, <https://doi.org/10.1029/2006JD007506>, 2007.
- 575 4. Anderson, M. C., Norman, J. M., Kustas, W. P., Houborg, R., Starks, P. J., and Agam, N.: A thermal-based remote
576 sensing technique for routine mapping of land-surface carbon, water and energy fluxes from field to regional scales,
577 112, 4227–4241, <https://doi.org/10.1016/j.rse.2008.07.009>, 2008.
- 578 5. Baldocchi, D., Falge, E., Gu, L., Olson, R., Hollinger, D., Running, S., Anthoni, P., Bernhofer, C., Davis, K., Evans, R.,
579 Fuentes, J., Goldstein, A., Katul, G., Law, B., Lee, X., Malhi, Y., Meyers, T., Munger, W., Oechel, W., U, K. T. P.,
580 Pilegaard, K., Schmid, H. P., Valentini, R., Verma, S., Vesala, T., Wilson, K., and Wofsy, S.: FLUXNET: A New Tool
581 to Study the Temporal and Spatial Variability of Ecosystem-Scale Carbon Dioxide, Water Vapor, and Energy Flux
582 Densities, 82, 2415–2434, [https://doi.org/10.1175/1520-0477\(2001\)082<2415:FANTTS>2.3.CO;2](https://doi.org/10.1175/1520-0477(2001)082<2415:FANTTS>2.3.CO;2), 2001.
- 583 6. Beven, K. J., Kirkby, M. J., Freer, J. E., and Lamb, R.: A history of TOPMODEL, *Hydrol. Earth Syst. Sci.*, 25, 527–
584 549, <https://doi.org/10.5194/hess-25-527-2021>, 2021.
- 585 7. Boulet, G., Mougnot, B., Lhomme, J.-P., Fanise, P., Lili-Chabaane, Z., Oliosio, A., Bahir, M., Rivalland, V., Jarlan, L.,
586 Merlin, O., Coudert, B., Er-Raki, S., and Lagouarde, J.-P.: The SPARSE model for the prediction of water stress and
587 evapotranspiration components from thermal infra-red data and its evaluation over irrigated and rainfed wheat, *Hydrol.*
588 *Earth Syst. Sci.*, 19, 4653–4672, <https://doi.org/10.5194/hess-19-4653-2015>, 2015.
- 589 8. Cerro, R. T. G. del, Subathra, M. S. P., Kumar, N. M., Verrastro, S., and George, S. T.: Modelling the daily reference
590 evapotranspiration in semi-arid region of South India: A case study comparing ANFIS and empirical models, 8, 173–
591 184, <https://doi.org/10.1016/j.inpa.2020.02.003>, 2021.
- 592 9. Chang, L.-L., Dwivedi, R., Knowles, J. F., Fang, Y.-H., Niu, G.-Y., Pelletier, J. D., Rasmussen, C., Durcik, M., Barron-
593 Gafford, G. A., and Meixner, T.: Why Do Large-Scale Land Surface Models Produce a Low Ratio of Transpiration to
594 Evapotranspiration?, 123, 9109–9130, <https://doi.org/10.1029/2018JD029159>, 2018.
- 595 10. Copernicus Climate Change Service (C3S): ERA5: Fifth generation of ECMWF atmospheric reanalyses of the global
596 climate. ERA5 hourly data on single levels from 1979 to present.: 10.24381/cds.adbb2d47, last access: 14 February
597 2020.
- 598 11. Efstratiadis, A. and Koutsoyiannis, D.: The multiobjective evolutionary annealing-simplex method and its application
599 in calibrating hydrological models, in: *Geophysical Research Abstracts, Conference: European Geosciences Union*
600 *General Assembly, Vienna, Austria*, <http://dx.doi.org/10.13140/RG.2.2.32963.81446>, 2005.
- 601 12. BROOK 90: A simulation model for evaporation, soil water, and streamflow.:
602 <http://www.ecoshift.net/brook/brook90.htm>, last access: 2 June 2021.
- 603 13. Feng, Y., Cui, N., Zhao, L., Hu, X., and Gong, D.: Comparison of ELM, GANN, WNN and empirical models for
604 estimating reference evapotranspiration in humid region of Southwest China, 536, 376–383,
605 <https://doi.org/10.1016/j.jhydrol.2016.02.053>, 2016.



- 606 14. Fisher, J. B., Melton, F., Middleton, E., Hain, C., Anderson, M., Allen, R., McCabe, M. F., Hook, S., Baldocchi, D.,
607 Townsend, P. A., Kilic, A., Tu, K., Miralles, D. D., Perret, J., Lagouarde, J.-P., Waliser, D., Purdy, A. J., French, A.,
608 Schimel, D., Famiglietti, J. S., Stephens, G., and Wood, E. F.: The future of evapotranspiration: Global requirements
609 for ecosystem functioning, carbon and climate feedbacks, agricultural management, and water resources, 53, 2618–
610 2626, <https://doi.org/10.1002/2016WR020175>, 2017.
- 611 15. Gupta, H. V., Kling, H., Yilmaz, K. K., and Martinez, G. F.: Decomposition of the mean squared error and NSE
612 performance criteria: Implications for improving hydrological modelling, 377, 80–91,
613 <https://doi.org/10.1016/j.jhydrol.2009.08.003>, 2009a.
- 614 16. Gupta, H. V., Kling, H., Yilmaz, K. K., and Martinez, G. F.: Decomposition of the mean squared error and NSE
615 performance criteria: Implications for improving hydrological modelling, 377, 80–91,
616 <https://doi.org/10.1016/j.jhydrol.2009.08.003>, 2009b.
- 617 17. Jung, M., Reichstein, M., Margolis, H. A., Cescatti, A., Richardson, A. D., Arain, M. A., Arneth, A., Bernhofer, C.,
618 Bonal, D., Chen, J., Gianelle, D., Gobron, N., Kiely, G., Kutsch, W., Lasslop, G., Law, B. E., Lindroth, A., Merbold,
619 L., Montagnani, L., Moors, E. J., Papale, D., Sottocornola, M., Vaccari, F., and Williams, C.: Global patterns of land-
620 atmosphere fluxes of carbon dioxide, latent heat, and sensible heat derived from eddy covariance, satellite, and
621 meteorological observations, 116, <https://doi.org/10.1029/2010JG001566>, 2011.
- 622 18. Kottek, M., Grieser, J., Beck, C., Rudolf, B., and Rubel, F.: World Map of the Köppen-Geiger climate classification
623 updated, 15, 259–263, <https://doi.org/10.1127/0941-2948/2006/0130>, 2006.
- 624 19. Kronenberg, R. and Bernhofer, C.: A method to adapt radar-derived precipitation fields for climatological applications,
625 22, 636–649, <https://doi.org/10.1002/met.1498>, 2015.
- 626 20. BROOK90 in R: https://github.com/rkronen/Brook90_R, last access: 2 June 2020.
- 627 21. Lawrence, D. M., Thornton, P. E., Oleson, K. W., and Bonan, G. B.: The Partitioning of Evapotranspiration into
628 Transpiration, Soil Evaporation, and Canopy Evaporation in a GCM: Impacts on Land–Atmosphere Interaction, 8, 862–
629 880, <https://doi.org/10.1175/JHM596.1>, 2007.
- 630 22. Leuning, R., Zhang, Y. Q., Rajaud, A., Cleugh, H., and Tu, K.: A simple surface conductance model to estimate
631 regional evaporation using MODIS leaf area index and the Penman-Monteith equation, 44,
632 <https://doi.org/10.1029/2007WR006562>, 2008.
- 633 23. Lide, D.: CRC Handbook of Chemistry and Physics, 85th ed., CRC Press, 2005.
- 634 24. Liu, M., Bárdossy, A., Li, J., and Jiang, Y.: Physically-based modeling of topographic effects on spatial
635 evapotranspiration and soil moisture patterns through radiation and wind, Hydrol. Earth Syst. Sci., 16, 357–373,
636 <https://doi.org/10.5194/hess-16-357-2012>, 2012.
- 637 25. Luong, T. T., Pöschmann, J., Vorobevskii, I., Wiemann, S., Kronenberg, R., and Bernhofer, C.: Pseudo-Spatially-
638 Distributed Modeling of Water Balance Components in the Free State of Saxony, 7,
639 <https://doi.org/10.3390/hydrology7040084>, 2020.



- 640 26. Mallick, K., Toivonen, E., Trebs, I., Boegh, E., Cleverly, J., Eamus, D., Koivusalo, H., Drewry, D., Arndt, S. K.,
641 Griebel, A., Beringer, J., and Garcia, M.: Bridging Thermal Infrared Sensing and Physically-Based Evapotranspiration
642 Modeling: From Theoretical Implementation to Validation Across an Aridity Gradient in Australian Ecosystems, 54,
643 3409–3435, <https://doi.org/10.1029/2017WR021357>, 2018.
- 644 27. Mauder, M., Genzel, S., Fu, J., Kiese, R., Soltani, M., Steinbrecher, R., Zeeman, M., Banerjee, T., De Roo, F., and
645 Kunstmann, H.: Evaluation of energy balance closure adjustment methods by independent evapotranspiration estimates
646 from lysimeters and hydrological simulations, 32, 39–50, <https://doi.org/10.1002/hyp.11397>, 2018.
- 647 28. McNally, A., McCartney, S., Ruane, A. C., Mladenova, I. E., Whitcraft, A. K., Becker-Reshef, I., Bolten, J. D., Peters-
648 Lidard, C. D., Rosenzweig, C., and Uz, S. S.: Hydrologic and Agricultural Earth Observations and Modeling for the
649 Water-Food Nexus, 7, 23, <https://doi.org/10.3389/fenvs.2019.00023>, 2019.
- 650 29. Miralles, D. G., Holmes, T. R. H., De Jeu, R. A. M., Gash, J. H., Meesters, A. G. C. A., and Dolman, A. J.: Global
651 land-surface evaporation estimated from satellite-based observations, 15, 453–469, [https://doi.org/10.5194/hess-15-](https://doi.org/10.5194/hess-15-453-2011)
652 453-2011, 2011.
- 653 30. Miralles, D. G., Jiménez, C., Jung, M., Michel, D., Ershadi, A., McCabe, M. F., Hirschi, M., Martens, B., Dolman, A.
654 J., Fisher, J. B., Mu, Q., Seneviratne, S. I., Wood, E. F., and Fernández-Prieto, D.: The WACMOS-ET project – Part 2:
655 Evaluation of global terrestrial evaporation data sets, *Hydrol. Earth Syst. Sci.*, 20, 823–842,
656 <https://doi.org/10.5194/hess-20-823-2016>, 2016.
- 657 31. Mueller, B., Seneviratne, S. I., Jimenez, C., Corti, T., Hirschi, M., Balsamo, G., Ciais, P., Dirmeyer, P., Fisher, J. B.,
658 Guo, Z., Jung, M., Maignan, F., McCabe, M. F., Reichle, R., Reichstein, M., Rodell, M., Sheffield, J., Teuling, A. J.,
659 Wang, K., Wood, E. F., and Zhang, Y.: Evaluation of global observations-based evapotranspiration datasets and IPCC
660 AR4 simulations, 38, <https://doi.org/10.1029/2010GL046230>, 2011.
- 661 32. Müller Schmied, H., Adam, L., Eisner, S., Fink, G., Flörke, M., Kim, H., Oki, T., Portmann, F. T., Reinecke, R.,
662 Riedel, C., Song, Q., Zhang, J., and Döll, P.: Variations of global and continental water balance components as
663 impacted by climate forcing uncertainty and human water use, *Hydrol. Earth Syst. Sci.*, 20, 2877–2898,
664 <https://doi.org/10.5194/hess-20-2877-2016>, 2016.
- 665 33. Murray, F. W.: On the Computation of Saturation Vapor Pressure, 6, 203–204, [https://doi.org/10.1175/1520-](https://doi.org/10.1175/1520-0450(1967)006<0203:OTCOSV>2.0.CO;2)
666 0450(1967)006<0203:OTCOSV>2.0.CO;2, 1967.
- 667 34. Nash, J. E. and Sutcliffe, J. V.: River flow forecasting through conceptual models part I — A discussion of principles,
668 10, 282–290, [https://doi.org/10.1016/0022-1694\(70\)90255-6](https://doi.org/10.1016/0022-1694(70)90255-6), 1970a.
- 669 35. Nash, J. E. and Sutcliffe, J. V.: River flow forecasting through conceptual models part I — A discussion of principles,
670 10, 282–290, [https://doi.org/10.1016/0022-1694\(70\)90255-6](https://doi.org/10.1016/0022-1694(70)90255-6), 1970b.
- 671 36. Pan, S., Pan, N., Tian, H., Friedlingstein, P., Sitch, S., Shi, H., Arora, V. K., Haverd, V., Jain, A. K., Kato, E., Lienert,
672 S., Lombardozzi, D., Nabel, J. E. M. S., Ottlé, C., Poulter, B., Zaehle, S., and Running, S. W.: Evaluation of global



- 673 terrestrial evapotranspiration using state-of-the-art approaches in remote sensing, machine learning and land surface
674 modeling, *Hydrol. Earth Syst. Sci.*, 24, 1485–1509, <https://doi.org/10.5194/hess-24-1485-2020>, 2020.
- 675 37. Reed, P. and Deviredy, V.: Groundwater monitoring design: a case study combining epsilon dominance archiving and
676 automatic parameterization for the NSGA-II, in: *Applications of Multi-Objective Evolutionary Algorithms*, 79–100,
677 https://doi.org/10.1142/9789812567796_0004, 2004.
- 678 38. Richter, D.: *Ergebnisse methodischer Untersuchungen zur Korrektur des systematischen Meßfehlers des Hellmann-*
679 *Niederschlagsmessers von Dieter Richter*, Deutscher Wetterdienst., Offenbach am Main, 1995.
- 680 39. Schulz, S., Becker, R., Richard-Cerda, J. C., Usman, M., aus der Beek, T., Merz, R., and Schüth, C.: Estimating water
681 balance components in irrigated agriculture using a combined approach of soil moisture and energy balance monitoring,
682 and numerical modelling, 35, e14077, <https://doi.org/10.1002/hyp.14077>, 2021.
- 683 40. Shuttleworth, W. J. and Wallace, J. S.: Evaporation from sparse crops-an energy combination theory, 111, 839–855,
684 <https://doi.org/10.1002/qj.49711146910>, 1985.
- 685 41. Spank, U., Schwärzel, K., Renner, M., Moderow, U., and Bernhofer, C.: Effects of measurement uncertainties of
686 meteorological data on estimates of site water balance components, 492, 176–189,
687 <https://doi.org/10.1016/j.jhydrol.2013.03.047>, 2013.
- 688 42. Vorobeuskii, I., Kronenberg, R., and Bernhofer, C.: Global BROOK90 R Package: An Automatic Framework to
689 Simulate the Water Balance at Any Location, 12, <https://doi.org/10.3390/w12072037>, 2020.
- 690 43. Wackernagel, H.: *Multivariate Geostatistics: an Introduction with Applications*, 3rd ed., Springer-Verlag, Berlin
691 Heidelberg, 388 pp., 2003.
- 692 44. Wei, Z., Yoshimura, K., Wang, L., Miralles, D. G., Jasechko, S., and Lee, X.: Revisiting the contribution of
693 transpiration to global terrestrial evapotranspiration, 44, 2792–2801, <https://doi.org/10.1002/2016GL072235>, 2017.
- 694 45. Winter, J. M. and Eltahir, E. A. B.: The Sensitivity of Latent Heat Flux to Changes in the Radiative Forcing: A
695 Framework for Comparing Models and Observations, 23, 2345–2356, <https://doi.org/10.1175/2009JCLI3158.1>, 2010.
- 696 46. Zeng, Z., Piao, S., Lin, X., Yin, G., Peng, S., Ciais, P., and Myneni, R. B.: Global evapotranspiration over the past three
697 decades: estimation based on the water balance equation combined with empirical models, 7, 014026,
698 <https://doi.org/10.1088/1748-9326/7/1/014026>, 2012.
- 699 47. Zhang, Y., Leuning, R., Hutley, L. B., Beringer, J., McHugh, I., and Walker, J. P.: Using long-term water balances to
700 parameterize surface conductances and calculate evaporation at 0.05° spatial resolution, 46,
701 <https://doi.org/10.1029/2009WR008716>, 2010.
- 702 48. Zink, M., Kumar, R., Cuntz, M., and Samaniego, L.: A high-resolution dataset of water fluxes and states for Germany
703 accounting for parametric uncertainty, *Hydrol. Earth Syst. Sci.*, 21, 1769–1790, <https://doi.org/10.5194/hess-21-1769->
704 2017, 2017.